Heliyon 9 (2023) e13086

Contents lists available at ScienceDirect

Heliyon

journal homepage: www.cell.com/heliyon

Research article

Characterisation and modelling the mechanics of cellulose nanofibril added polyethersulfone ultrafiltration membranes

Seren Acarer [a], İnci Pir [b], Mertol Tüfekci [c,*], Tuğba Erkoç [d], Vehbi Öztekin [b], Sevgi Güneş Durak [e], Mehmet Şükrü Özçoban [f], Güler Türkoğlu Demirkol [a], Moayyad Alhammod [a], Selva Çavuş [d], Neşe Tüfekci [a]

[a] Istanbul University-Cerrahpasa, Faculty of Engineering, Department of Environmental Engineering, Avcilar, 34320 Istanbul, Turkey
[b] Istanbul Technical University, Faculty of Mechanical Engineering, Istanbul 34437, Turkey
[c] Imperial College London, Department of Mechanical Engineering, South Kensington Campus, Exhibition Road, London SW7 2AZ, UK
[d] Istanbul University-Cerrahpaşa, Faculty of Engineering, Department of Chemical Engineering, Avcilar, 34320 İstanbul, Turkey
[e] Nevsehir Haci Bektas Veli University, Department of Environmental Engineering, Faculty of Engineering-Architecture, Nevsehir 50300, Turkey
[f] Yıldız Technical University, Faculty of Civil Engineering, Davutpaşa, 34220, İstanbul, Turkey

ARTICLE INFO

Keywords:
Nanocomposite membrane
Membrane characterisation
Cellulose nanofibril
Mechanical modelling

ABSTRACT

The performance of the membranes can be improved by adding the appropriate amount of nanomaterials to the polymeric membranes that can be used for water/wastewater treatment. In this study, the effects of polyvinylpyrrolidone (PVP), the impact of different amounts (0.5% and 1% wt.) of cellulose nanofibril (CNF), and the combined effects of PVP-CNF on the properties/performance of the polyethersulfone-based (PES-based) membrane are investigated. All PES-based ultrafiltration (UF) membranes are manufactured employing the phase inversion method and characterised via Fourier transform infrared (FTIR) spectroscopy, scanning electron microscopy (SEM), and the relevant techniques to determine the properties, including porosity, mean pore size, contact angle, water content, and pure water flux tests. Furthermore, the thermal properties of the prepared membranes are investigated using thermal gravimetric analysis (TGA) and differential thermal analysis (DTA) techniques. Experimental and numerical methods are applied for the mechanical characterisation of prepared membranes. For the experimental process, tensile tests under dry and wet conditions are conducted. The finite element (FE) method and Mori-Tanaka mean-field homogenisation are used as numerical methods to provide more detailed knowledge of membrane mechanics.

1. Introduction

PES is one of the polymers widely used in membrane preparation due to its superior properties, like better chemical and thermal resistance, being able to be used in a wide pH range, and enabling membrane preparation in different configurations and pore sizes [1, 2].

Natural reinforcements are also becoming more widely used since they do not pose significant health risks, especially for water treatment applications [3]. Cellulose is a natural and renewable polymer abundant on earth, with an average production of 10^9 tons

* Corresponding author.
E-mail address: m.tufekci17@imperial.ac.uk (M. Tüfekci).

https://doi.org/10.1016/j.heliyon.2023.e13086
Received 14 September 2022; Received in revised form 12 January 2023; Accepted 16 January 2023
Available online 21 January 2023

per year [4–6]. Nanocelluloses are materials obtained from cellulose and have at least one dimension at the nanometre level (1–100 nm) [7]. The outstanding properties of nanocellulose include small size, high aspect ratio and specific surface area, high stiffness, low density, non-toxicity, biodegradability, and sustainability [8–12]. Nanocellulose materials are divided into three primary classes cellulose nanofibril (CNF), cellulose nanocrystal (CNC), and bacterial cellulose (BC) [13]. Cellulose nanofibril (CNF) is a type of nanocellulose with a diameter of 5–100 nm and a length of up to a few micrometres [13], which is obtained by subjecting cellulose fibres to mechanical processes such as homogenisation, grinding and milling [14,15]. Several hydroxyl groups which can be found on the surface of CNF [16,17] contribute to the increase of membrane hydrophilicity by incorporating CNF into the polymeric membrane matrix [18]. In addition, the high modulus (~78 GPa) and tensile strength (~4 GPa) of CNFs make them good candidates for reinforcement materials for enhancing the mechanical behaviour of polymers [19].

Many researchers have reported that the hydrophilicity [20–29], pure water flux [20,22–24,26–33], mechanical strength [20,22,24,26,27,34,35], porosity [20,24,27,28,31,35], pore size [20,24,27–29,35], contaminant removal efficiency [22,23,29,32] and fouling resistance [23,35] of the membranes rise with the addition of nanocellulose to polymeric membranes. Qu et al. show that adding 1% CNF to the PES membrane increases the pure water flux by 1.36 times and improves the membrane mechanical behaviour by increasing the tensile strength and elongation at break to 7.25 MPa and 11.6%, respectively [24]. Ding et al. report that the tensile strength of a 0.8% CNF-doped polysulfone membrane increases from 158 MPa to 391 MPa compared to a neat polysulfone membrane [27]. Battirola et al. report that the pure water flux of the cellulose acetate (CA) membrane prepared by the phase inversion method increased from 40 L/m^2. h to 940 L/m^2. h with the addition of 10% CNF [31]. Similarly, Li et al. show that the pure water flux of the CA membrane increased 7-fold from 15 L/m^2. h to 102 L/m^2. h with the addition of 0.3% CNF [33]. In the study by Kong et al., it is determined that the pure water flux of the cellulose triacetate (CTA) membrane doped with 1.5% 2,2,6,6 tetramethylpiperidine-1-oxyl (TEMPO)-oxidised CNF (TOCN) membrane (224.68 L/m^2. h) is found to be higher than the pure CTA membrane (90.57 L/m^2. h) [35].

Polyvinylpyrrolidone (PVP) is a biocompatible [36,37], non-toxic [37] and biodegradable [37] polymer. PVP also has outstanding optical, electrical properties and mechanical properties [36], perfect film-forming capability [37,38] and water solubility [36–38]. In addition to solubility in water, it exhibits solvent solubility having different polarity, and its excellent binding and stabilising nature contribute to its superior properties [37]. It is stated that the amphiphilic character of PVP can affect morphology [38]. It can be preferred as an important additive in the membrane preparation process because of its good pore former function [39–41]. It is reported that the hydrophilicity of the membrane surface is improved using PVP [39,41], increasing the membrane performance [39]. Marino et al. (2019) study the effect of PVP and Pluronic® additives on the performance of polyethersulfone membranes. It is stated that the thickness and mechanical strength of the membrane increase when PVP is used [42]. Ren et al. (2018) reveal that the conductivity and mechanical strength of the membranes improved when the membranes of aromatic polymers such as polyethersulfone and polysulfone are prepared with PVP [43].

It is possible to determine the mechanical properties of materials through various experimental methods. Tensile tests and dynamic mechanical analysis are examples of these experimental methods [20,44–49]. In addition, several researchers have studied the hygrothermal properties of composite materials [50,51]. In similar studies, different mechanical behaviours of wet and dry membranes are investigated, and it is observed that dry samples are found to be more rigid compared to wet samples [24,52,53]. In this direction, wet and dry conditions can be taken into account while performing the mechanical characterisation of the membranes.

Experimental methods are used to study the mechanical behaviour of a material under certain conditions. Furthermore, the effect of reinforcement material on mechanical properties can be determined by experimental methods in various reinforcement combinations in composites [54,55]. The tensile test can be given as an example of these experimental methods. The tensile test is one of the standard and commonly preferred methods because it is straightforward to perform and yields consistent results. In the tensile test, a uniaxial load is applied to the specimen. From the results obtained from the experiments, stress-strain diagrams of the material can be drawn, and the material's Young's modulus and elongation at break values can be extracted. From obtained data, the mechanical behaviour of the tested material can be interpreted.

In addition, preparing polymer matrix membrane samples, conducting the experiments and evaluating the test results is time-consuming and resource-intensive. To this extent, numerical modelling methods have a significant impact on developing particle-reinforced materials [56–58]. In numerical modelling, materials are assumed homogeneous and isotropic to facilitate calculations and analyses. In the literature, various methods exist for modelling composite materials. Mori-Tanaka-mean field homogenisation and finite element (FE) methods can be examples of conducting composite material's mechanical behaviour [59–61]. Here, the assumption is made that the matrix is an elastoplastic and the reinforcements are purely elastic materials. Quick and easy results can be obtained in the Mori-Tanaka method, and the elastic modulus of the composite material can be obtained in light of the components that make up the composite material. In addition to determining the modulus of elasticity using the FE method, which also enables one to simulate the damages that occur in the matrix also interface of particle reinforcement and the matrix [59].

In this study, PES, PES-PVP, PES-CNF and PES-PVP-CNF membranes are fabricated using the phase inversion method and then characterised experimentally aiming to explore the effects of the presence of CNF in various amounts (0.5% and 1% CNF wt.) on the chemical fingerprint, morphology, porosity, mean pore size, hydrophilicity, pure water flux, thermal properties, and mechanical properties of PES and PES-PVP membranes are investigated. The contributions of our study to the literature are as follows: First of all, to the best of the authors' knowledge, no study is spotted comparing the effects of CNF at different rates on PES and PES-PVP membranes, which are widely used in water and wastewater treatment, together. Secondly, the effect of CNF on the thermal properties of PES and PES/PVP membranes is investigated in detail, contrary to the thermal analysis in the literature, which is underestimated in membrane characterisation studies. Moreover, since the mechanical strength of pressure-driven water/wastewater treatment membranes is desired to be used for a longer time, this study provides detailed results on the effect of CNF additive on the mechanics of PES-based UF membranes with numerical methods, which are lacking in research in the literature, in addition to

experimental studies. Detailed findings of PVP addition, CNF addition, and co-addition of both PVP and CNF to PES membranes allow the detection of membranes with better water flux, mechanical stability, and thermal stability. Thus, membranes that are more resistant to thermal and mechanical effects and have higher flux performance can be selected appropriately for water/wastewater treatment. Hence the membranes can be operated for a longer time and at less cost.

2. Materials and methods

2.1. Materials

PES (VERADEL® 3000P), with an average molecular weight of 63,000 g/mol, is obtained from Solvay Specialty Polymers (Belgium). PVP (molecular weight of 40,000 g/mol in average) is obtained from Sigma-Aldrich. N-Methyl-2-Pyrrolidone (NMP, EMPLURA®) of $\geq$99.5% purity is obtained from Merck. CNF is purchased from Nanografi Nanotechnology (Turkey). CNF has a moisture content of 4% wt. The width and length of CNF are known as 10–20 nm and 2–3 μm, respectively.

2.2. Membrane preparation

PES, PES-PVP, PES-CNF, and PES-PVP-CNF flat sheet membranes are prepared by the phase inversion method. The composition of the prepared membranes is given in Table 1. The amount of PES in all membranes is kept constant at 16% wt.

The required amount of CNF is added to the NMP solvent and dispersed in a heated magnetic stirrer (WiseStir MSH-20A) for 10 min at 60 °C at a high stirring speed. Then, 8% wt. of PVP is added, and the solution is stirred until the PVP is completely dissolved (approximately 2 h). In the next step, 16% wt. of PES is added, and the membrane casting solution is mixed at 60 °C for 24 h until a homogeneous mixture is obtained. An ultrasonic bath (Weightlab Instruments) process is applied at 25 °C for 30 min to remove the bubbles in the casting solution and to distribute the CNF homogeneously in the solution. Membrane casting solutions are cast on a plate made of glass using a blade (TQC Sheen, VF2170-261, 200 μm). Membrane films are immersed in a coagulation bath with distilled water as well as the plate made of glass. After about 2 min, the polymeric membranes rise to the water surface in the coagulation bath. These prepared membranes are stored in distilled water at 4 °C until used in characterisation studies. PES, PES-PVP, and PES-CNF membranes are prepared using the same procedure.

2.3. Membrane characterisation

2.3.1. FTIR spectroscopy

The FTIR analysis is carried out on a PerkinElmer Spectrum 100 in the range of 650–4000 cm^{-1}.

2.3.2. Thermal characterisation

Thermal behaviour of the membranes is investigated using a DTA-TGA apparatus (Shimadzu DTG-60) under a nitrogen atmosphere with a heating rate of 10 °C min^{-1} and temperature range of 25 °C–800 °C.

2.3.3. SEM

The morphology of the manufactured membranes are visualised with SEM (FEI Quanta 250 FEG) operating at a 20 kV acceleration voltage. The samples are covered/coated with a layer of gold before they are put through SEM analysis to acquire the images of the samples' surface and cross-section. Surface and cross-section images of the membranes are obtained at 5000× and 1500× magnifications, respectively.

2.3.4. Contact angle

The contact angle is obtained through the measurement of the angle between the membrane surface and distilled water dripped with a syringe onto the membrane using a goniometer (KSV CAM 101). Contact angles are measured at room temperature (25 °C). Contact angle measurements are repeated until at least three sets of consistent results for each membrane sample are acquired and these results are averaged.

Table 1
The material composition of the manufactured membranes.

Membrane Type	PES (wt. %)	NMP (wt. %)	PVP (wt. %)	CNF (wt. %)
PES	16	84	–	–
PES-CNF0.5	16	83.5	–	0.5
PES-CNF1	16	83	–	1
PES-PVP	16	76	8	–
PES-PVP-CNF0.5	16	75.5	8	0.5
PES-PVP-CNF1	16	75	8	1

2.3.5. Water content

All membranes are prepared in uniform size to determine the membranes' water content. First, the membranes are dried in a 60 °C oven (Nuve EN 500) for 24 h, and their dry weights are determined with a precision balance (Kern 573). Then, the membranes are dipped/bathed in water, and the weights of the wet membranes are measured following the removal of the excess water on the membrane samples using drying paper. The membranes' water content is found according to Eq. (1) using the weights of the membranes in wet and dry conditions:

$$\text{Water content } (\%) = \frac{W_w - W_d}{W_w} \text{ x } 100 \tag{1}$$

W_w and W_d denote the wet and dry weights (g) of the membrane samples.

2.3.6. Porosity

The porosity (ε) of the membranes is determined by the gravimetric method and calculated using Eq. (2).

$$\varepsilon\ (\%) = \frac{W_w - w_d}{A\ l\ \rho} \text{x } 100 \tag{2}$$

where, W_w, W_d, A, and l are the wet and dry weights (g), surface area (cm^2), and thickness (cm) of the membrane, respectively. Meanwhile, "ρ" denotes the water's density which is given as 0.998 g/cm^3.

2.3.7. Mean pore size

The mean pore size (rm) of the membrane samples is determined with the Guerout-Elford-Ferry Equation that is presented in Eq. (3).

$$r_m = \sqrt{\frac{(2.9 - 1.75\varepsilon) \text{ x } 8\eta l Q}{\varepsilon \text{ x } A \text{ x } \Delta P}} \tag{3}$$

where ε is the porosity, l is the thickness (m), A is the effective area (m^2) of the membrane sample, η is the viscosity of water (8.9×10^{-4} Pa s), Q is the volume of permeate water per unit time (m^3/s), and ΔP is the operating pressure (0.3 MPa).

2.3.8. Pure water flux

Pure water flux measurements are performed on the membrane samples in a dead-end filtration cell (Tin Mühendislik, Turkey) using nitrogen gas (N_2) as the driving force. The effective area of the membranes is 19.62 cm^2. Pure water is passed through the membranes at 3 bars under steady conditions, and the flux profile is transferred to the computer depending on time. The flux calculation for the membranes is made using Eq. (4).

$$J = \frac{V}{A\Delta t} \tag{4}$$

Here, J is the flux (L/m^2. h), V is the permeate volume (L), A is the effective area of the membrane sample (m^2), and Δt is the time (h).

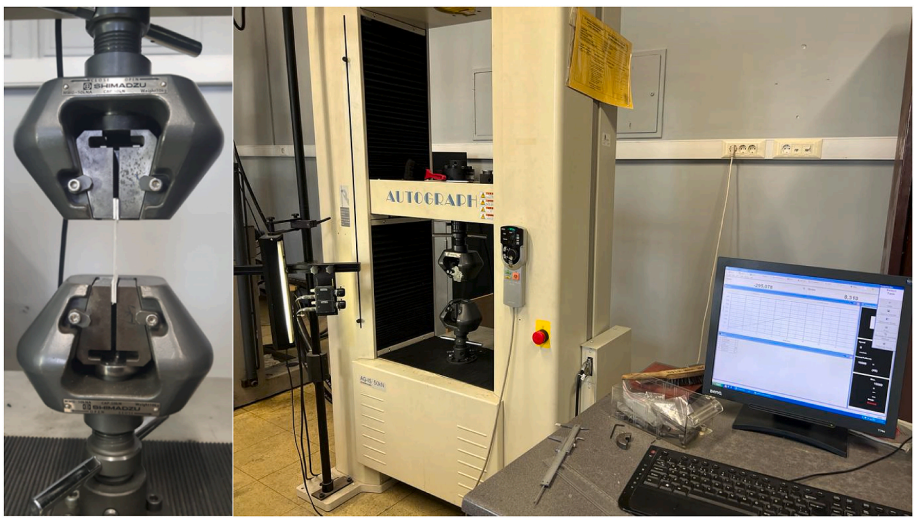

Fig. 1. Test specimen/testing equipment.

2.4. Mechanical properties of the membranes

In this section, the mechanical properties of membranes are obtained by employing experimental and numerical methods. Firstly, for the experimental part of this study, tensile tests are conducted. After the experimental stage, Mori-Tanaka mean field homogenisation and FE analysis are performed for numerical investigations.

2.4.1. Tensile tests

Within the scope of this study, tensile tests are carried out on PES/NMP wet and dry membranes, PES/PVP wet and dry membranes, and the combinations of these membranes with 0.5% and 1% CNF reinforcement by weight in wet and dry conditions. The Shimadzu AG-IS 50 kN universal test machine is used to perform tensile tests on the membranes. For quasi-static testing, the strain rate is maintained constant and is less than 1% strain per minute. Aluminium plates are glued to the membrane specimens' tips to prevent slippage when being clamped and tested. Each membrane is put through the test as wet and dry. The drying is done at room temperature as air drying that lasts 24 h. At least three tests are done for each membrane combination to ensure consistency and repeatability. Test specimen/testing equipment is shown in Fig. 1.

2.4.2. Numerical modelling

Mori-Tanaka mean-field homogenisation and the FE methods are commonly used to calculate the mechanical properties using the properties of the individual materials of which the composite material consists. For this study, the matrix (PES) and the inclusion (CNF) are assumed to be linear elastic, and only the linear elastic region of those materials is of interest. These mechanical properties are determined using the tensile tests conducted within the scope of this study. Hence, a representative volume element (RVE) is constructed with randomly chosen positions of the particle inclusions. This RVE is put through a uniaxial strain alongside periodic boundary conditions (PBC). For the calculations. For the same purpose as Mori-Tanaka, FE analysis is also performed on an RVE. Assuming the periodicity of the RVE, the FE model is solved using commercial software. Due to the periodicity assumption, the RVE sizes and content must be selected and generated carefully. No doubt should be there about its capability to represent the material with its structure. The RVE is strained uniaxially in the tensile direction with a maximum displacement that corresponds to a strain of 0.03 on one surface with PBC. The RVE presentation of the CNF-reinforced composite structure is in Fig. 2.

3. Results

3.1. FTIR of the membranes

The chemical structure of the prepared membranes is analyzed by FTIR. The FTIR spectra of the membranes in the range of 4000–650 cm^{-1} are shown in Fig. 3. In the spectrum of neat PES, the peak observed at 3096 cm^{-1} (C–H stretching) is due to an

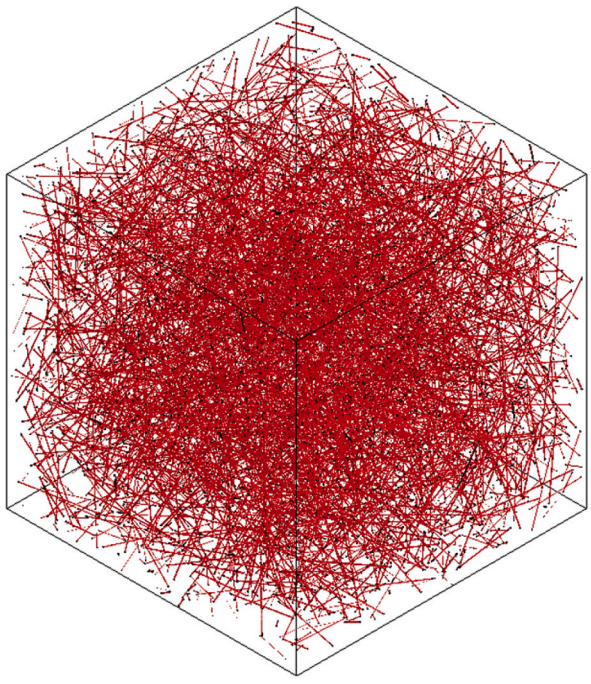

Fig. 2. RVE presentation of CNF reinforced composite structure.

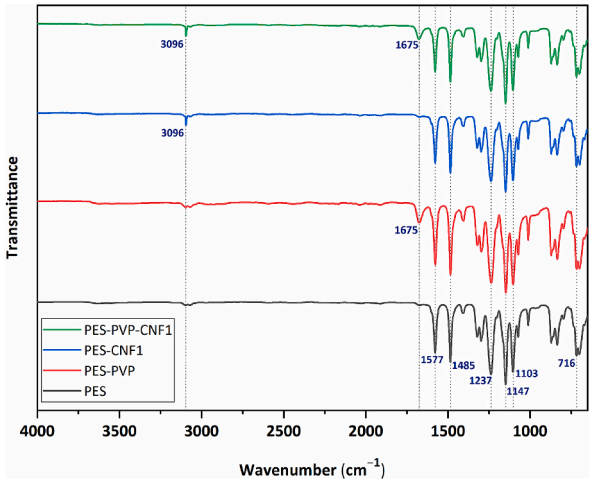

Fig. 3. FTIR spectra of membranes.

aromatic ring [62,63]. The C]C stretching vibration of the aromatic benzene ring can be seen at 1485 and 1577 cm^{-1} [62,63]. The presence of ether linkage (C–O–C stretching) is confirmed by the peak at 1237 cm^{-1} [62,63]. The peaks observed at 1147 [62,63] and 1103 cm^{-1} [63] correspond to the sulfone group (O]S]O). The C–S stretching vibrations are observed at 716 cm^{-1} [62]. In the FTIR spectra of PES-PVP and PES-PVP-CNF1, a new peak due to the carbonyl (C]O) group of PVP [64] is observed at 1675 cm^{-1} confirming the presence of PVP in the membrane. CNF-containing membranes have more prominent and less intense peaks at 3096 and 1577 cm^{-1}, respectively. The more intense peaks at 3096 cm^{-1} can be assigned to the additional effect of the C–H stretching vibration of CNF.

3.2. *Thermal behaviour of the membranes*

Although the rise in the water/wastewater temperature passing through the membranes contributes positively to the growth in the flux performance of the membrane, prolonged exposure of the membranes to the high-temperature feed water/wastewater causes their structure to deteriorate. For this reason, the high thermal stability of membranes used in water/wastewater treatment is desired. Thermal behaviours of the prepared membranes are analyzed, and the effects of the presence of PVP and the amount of CNF on the weight loss percentage, maximum decomposition temperature and thermal stability are determined. The thermogravimetric curves of PES, PES-CNF0.5, PES-CNF1, PES-PVP, PES-PVP-CNF0.5, PES-PVP-CNF1 membranes, and CNF are depicted in Fig. 4. The percentages of the decrease of weight at different temperatures and the values of maximum decomposition temperatures (T_{max}) can be seen in Tables 2 and 3, respectively. The maximum decomposition temperature of the PES membrane is found to be 562.4 °C according to the first derivative of TGA (DTG figure is not given here), and 10.5% (500 °C), 48.5% (600 °C), 60.4% (700 °C) and 74.0% (800 °C) weight losses of the PES membrane are observed. Abdul Mannan et al. (2016) report that the initial and final degradation temperatures of the PES membrane are 522.70 °C and 579.15 °C, respectively [65]. It is also stated that PES showed decomposition in the range of 580°C–600 °C [41]. The DTA exothermic peak of PES is observed at around 580 °C, as shown in Fig. 4a. It is previously reported that the DTA exothermic peak of pure PES is 562 °C [66].

CNF's initial thermal degradation temperature is given as 273 °C [31]. Ulrich and Faez et al. found that the thermodegradation of CNF takes place in one stage at 349 °C (maximum temperature, degradation), associated with the breakdown of glucose units. And also, depolymerisation, dehydration, oxidation, and carbonised residue decomposition are included in the degradation process [67]. In the study by Cao et al. the weight loss for CNF is observed as between 440°C and 800 °C is attributed to the fibre residue carbonisation in the N_2 environment [68]. Fig. 4b initially shows a 3.1% weight loss, probably due to the moisture and volatile products between 30°C and 100 °C. The maximum temperature (degradation) and the decomposition peaks are found at 314 °C and 639 °C, respectively (Fig. 4b). When the crystallinity degree of CNF is high, it provides higher heat resistance and greater thermal stability [69]. The weight losses of CNF are 5.7, 27.9, 53.4, 57.8, 58.5 and 78.2% at 200 °C, 300 °C, 400 °C, 500 °C, 600 °C, and 700 °C, respectively. The residue at 800 °C of CNF is about 19.3%. Higher CNF content in the PES membrane increases thermal stability. The highest thermal stability is observed in PES-CNF1, and the weight loss became 68.4% at 800 °C. The weight losses of PES-CNF1 are 8.0% (500 °C), 36.8% (600 °C), and 52.7% (700 °C). However, incorporating less CNF into PES has the opposite effect resulting in a decrease in thermal stability. The weight loss of PES-CNF0.5 is 91.8 at 800 °C. The decomposition of the carbonised residue is determined as 650 °C and 682 °C for PES-CNF0.5 (Fig. 4c) and PES-CNF1 (Fig. 4d), respectively.

The decomposition temperature of PVP is reported to be around 440 °C [41,70]. The presence of PVP in membranes decreases thermal stability since the decomposition temperature of PVP is lower than the decomposition temperature of PES [41]. In the current study, the thermal stability and the maximum decomposition temperature of PES-PVP-CNF1 are remarkably reduced compared to PES-CNF1. The weight losses of PES-PVP-CNF1 are 9.6, 16.4, 53.5, 74.5 and 94.5% at 400 °C, 500 °C, 600 °C, 700 °C, and 800 °C,

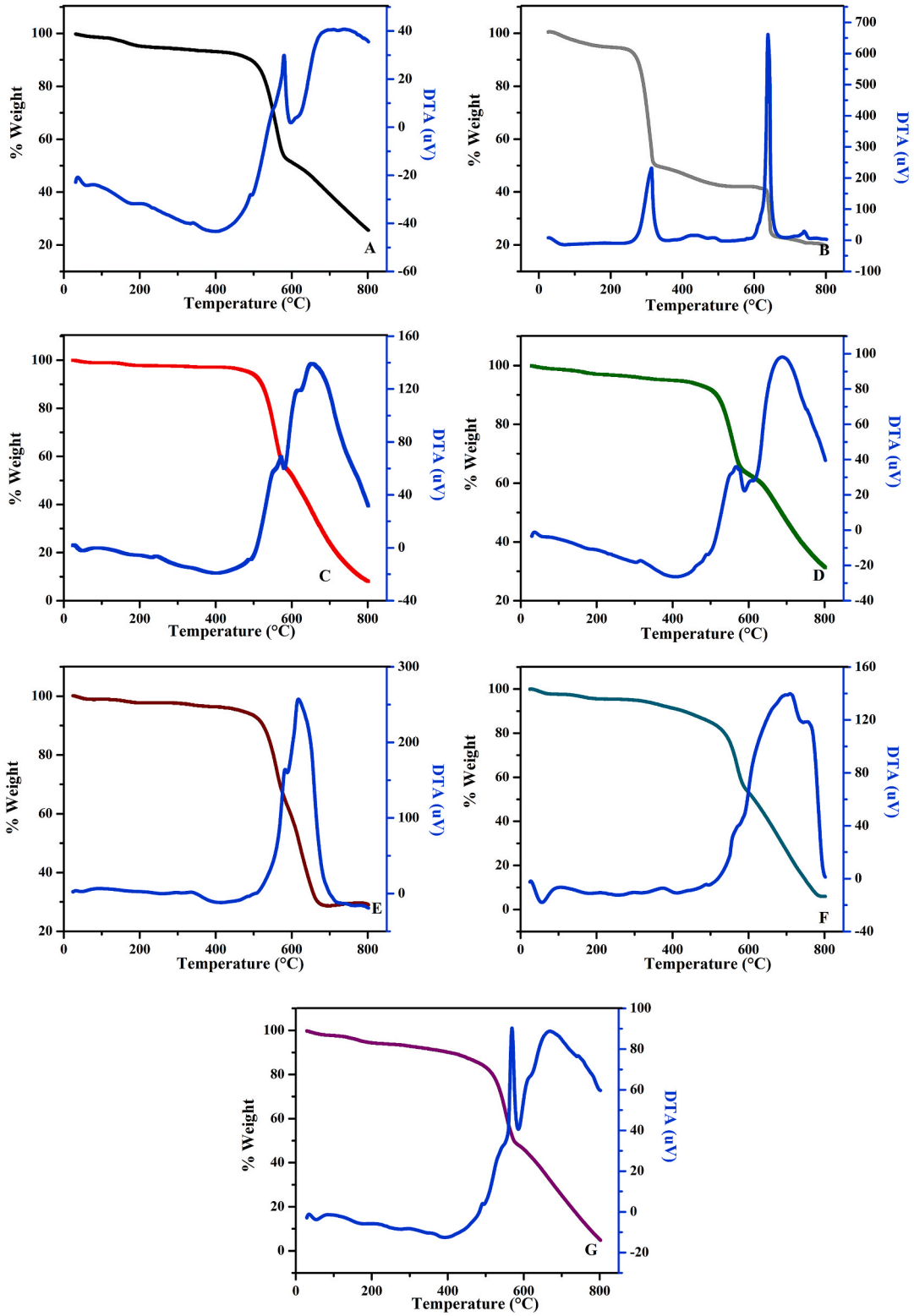

Fig. 4. Thermogravimetric curves of PES (A), CNF (B), PES-CNF0.5 (C), PES-CNF1 (D), PES-PVP (E), PES-PVP-CNF0.5 (F) and PES-PVP-CNF1 (G).

respectively, and the maximum decomposition temperature of PES-PVP-CNF1 is 544.1 °C (Table 3). The weight losses of PES-PVP-CNF0.5 are 8.6, 14.9, 46.8, 73.2 and 93.9% at 400 °C, 500 °C, 600 °C, 700 °C, and 800 °C, respectively. The residual amount of PES-PVP (Fig. 4e) is higher than those of PES-PVP-CNF0.5 (Fig. 4f) and PES-PVP-CNF1 (Fig. 4g). It is stated that the addition of CNF increased the rate of weight loss [71]. Ulrich and Faez et al. evaluate the thermal behaviour of composite films containing cellulose nanofiber, and it is stated that after the temperature at which CNF shows complete thermal degradation (400 °C), the higher CNF composites concentration caused greater mass loss. Moreover, it is reported that the maximum temperature (degradation) value also decreases after the addition of CNF [67]. The maximum peak is found at 665 °C for PES-PVP-CNF1 due to the carbonised residue decomposition, as shown in DTA (Fig. 4g).

3.3. Membrane morphology

The porosity, the size of the pores and the shape of the pores on the surface, and the internal structure of the membranes used in water/wastewater treatment are effective on the flux and contaminant removal performance of the membrane. Fig. 5 shows the SEM surface and cross-sectional images of the membranes. All membranes are porous and asymmetrical. The combination of PVP, CNF, and PVP-CNF in the PES membrane causes a change in the appearance of finger-like spaces extending from the surface of the PES membrane to the substrate.

3.3.1. Effect of PVP on membrane morphology

PVP, a hydraulic polymer, is widely used to prepare membranes used in water treatment to increase the membrane porosity and facilitate the water passage through the membrane [72,73]. Larger pores appear on the surface of the PES-PVP membrane (Fig. 5d) compared to the neat PES membrane (Fig. 5a). Since PVP is a water-soluble polymer, while there is an exchange between solvent (NMP) and water in the process of phase-inversion, the pore size of the membrane increases as a result of PVP moving from one point to another [72]. On the other hand, the upper layer of PES-PVP becomes denser than PES, and the finger-like spaces in PES are replaced by macro voids in the middle and lower layers. This may be attributed to the more viscous character of the PES-PVP casting solution than the PES casting solution.

3.3.2. Effect of CNF on membrane morphology

With the contribution of CNF to the PES membrane, the porosity and size of the pores on the surface of the membranes increases. The increase in porosity and pore size is due to the rise of CNF to the surface during the process of phase inversion, and the O–H groups in its structure increase the exchange rate between solvent and water [26]. When the amount of CNF in the PES casting solution rises from 0.5% to 1% wt., the number of pores on the membrane surface increase, and a more porous structure is obtained throughout the membrane's internal structure. The presence of more O–H groups due to adding more CNF into the membrane structure increases the exchange rate between non-solvent and solvent during membrane preparation, thus contributing to the increase in porosity and pore size.

Table 2
Weight loss at different temperatures.

Weight loss percentages								
Membrane type	100 °C	200 °C	300 °C	400 °C	500 °C	600 °C	700 °C	800 °C
PES	1.3	4.5	5.6	6.6	10.5	48.5	60.4	74.0
CNF	3.1	5.7	27.9	53.4	57.8	58.5	78.2	80.7
PES-CNF0.5	0.9	2.1	2.4	2.8	5.8	47.7	75.9	91.8
PES-CNF1	1.1	2.8	3.7	4.9	8.0	36.8	52.7	68.4
PES-PVP	1.3	2.4	2.6	3.9	6.8	41.3	71.6	71.1
PES-PVP-CNF0.5	2.3	4.4	4.9	8.6	14.9	46.8	73.2	93.9
PES-PVP-CNF1	2.1	5.4	6.8	9.6	16.4	53.5	74.5	94.5

Table 3
Maximum decomposition temperatures (T_{max}) of prepared membranes.

Membrane type	T_{max} (°C)
PES	562.4 °C
PES-CNF0.5	558.4 °C
PES-CNF1	561.9 °C
PES-PVP	562.8 °C
PES-PVP-CNF0.5	571.0 °C
PES-PVP-CNF1	544.1 °C

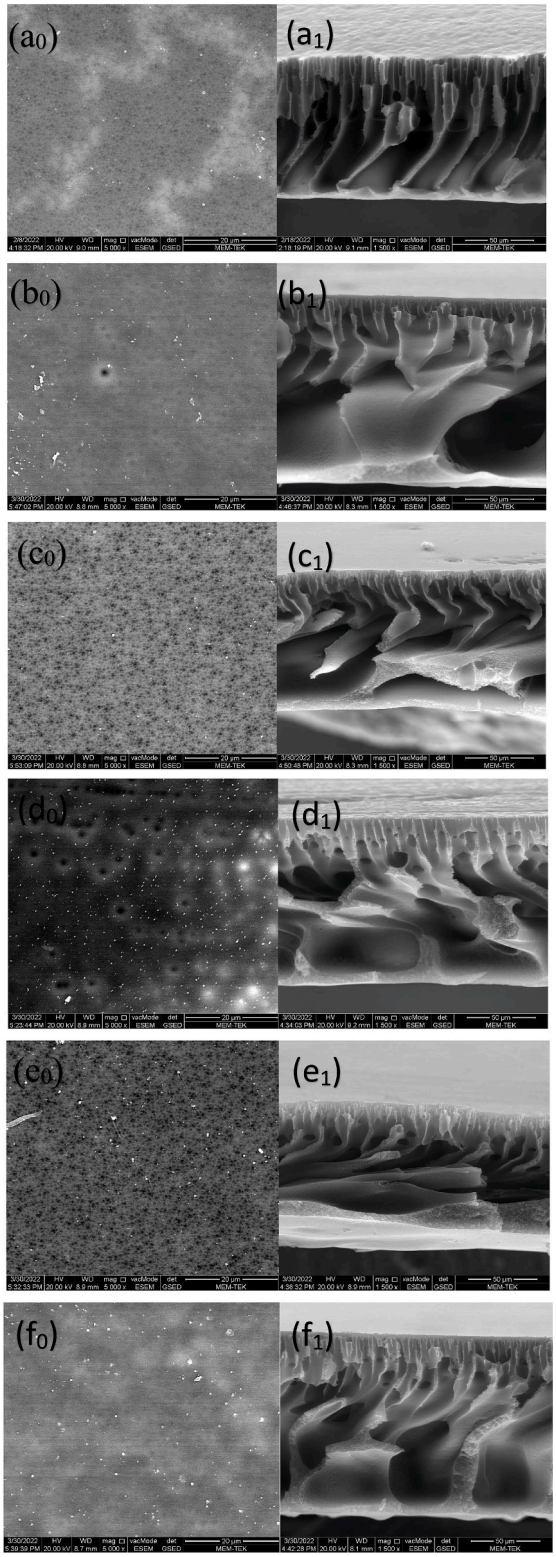

Fig. 5. SEM surface and cross-sectional views of the membranes (a) PES, (b) PES-CNF0.5, (c) PES-CNF1, (d) PES-PVP, (e) PES-PVP-CNF0.5, (f) PES-PVP-CNF1.

3.3.3. Effect of PVP-CNF on membrane morphology

From the SEM surface views, the surface porosity of the PES-PVP-CNF0.5 membrane (Fig. 5e) is higher than that of the PES (Fig. 5a), PES-PVP (Fig. 5d), and PES-CNF0.5 membrane (Fig. 5b). This proves that the synergistic effect of 8% wt. of PVP and 0.5% of CNF is more effective in increasing porosity than when adding 8% wt. of PVP or 0.5% wt. of CNF separately. However, the PES-PVP-CNF1 membrane (Fig. 5f) not only has a denser surface than the PES, PES-PVP, and PES-CNF1 (Fig. 5c) membranes but also has a denser internal structure. This can be explained by the fact that PVP and the high additive of CNF (1% wt.) excessively increase the viscosity of the membrane casting solution. The high PES-PVP-CNF1 casting solution lowers the rate of change during phase inversion, delaying the liquid-liquid separation and forming a less porous, denser membrane [35,74,75]. Similarly, the structure of PES-PVP-CNF1 is denser than PES-PVP-CNF0.5 due to the high loading of CNF increasing the membrane viscosity.

3.4. Membrane surface hydrophilicity

The hydrophilicity of the membrane surface is characterised by measuring the contact angle. A low contact angle means high hydrophilicity of the membrane surface. In Fig. 6, the contact angle of the membranes is shown.

3.4.1. Effect of PVP on membrane surface hydrophilicity

The membrane material which has the most hydrophobic surface is PES, with the greatest contact angle (94°). By incorporating the hydrophilic PVP into the hydrophobic PES, the contact angle decreases to 85°, and a more hydrophilic membrane is obtained. Similarly, Junaidi et al. report that their study shows that the contact angle decreases when PVP is added to the PES membrane casting solution [76]. It is known in the literature that the contact angle decreases as the membrane surface porosity and/or pore size increases [46]. The formation of larger pores on the surface of PES-PVP compared to PES (Fig. 5) allows water to spread more easily on the surface of the membrane samples and contributes to the climb in hydrophilicity.

3.4.2. Effect of CNF on membrane surface hydrophilicity

The contact angle of the membranes made of PES with CNF inclusions is lower compared to unreinforced PES membranes. CNF contributes to the improvement of membrane surface hydrophilicity due to the increased affinity between water and hydroxyl (-OH)

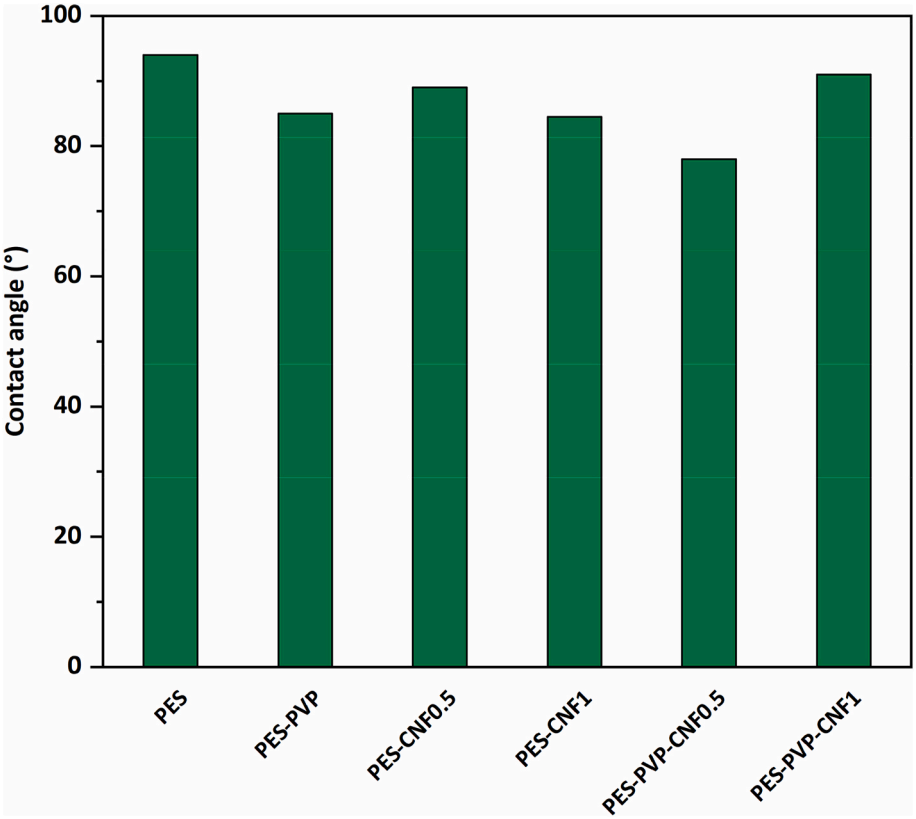

Fig. 6. The measured and averaged contact angles of the membrane samples.

groups, which are abundant in their structure [26]. Also, the contact angle of the PES membrane gradually decreases with the increase of CNF addition from 0.5% to 1% wt. Since more CNF means more –OH groups in the membrane matrix, adding 1% wt. of CNF results in a tremendous increase in membrane hydrophilicity. In addition, PES-CNF1 with the highest surface porosity among PES, PES-CNF0.5, and PES-CNF1 has the lowest contact angle, which shows the agreement between SEM surface images and contact angle results.

3.4.3. Effect of PVP-CNF on membrane surface hydrophilicity

The surface of the PES-PVP-CNF0.5 membrane is more hydrophilic than the surface of PES, PES-PVP, and PES-CNF0.5 membranes. In other words, the synergistic effect of 8% wt. of PVP and 0.5% wt. of CNF in the membrane provided superior performance in building up the hydrophilicity of the membrane compared to the effect of both materials alone. On the other hand, the PES-PVP-CNF1 membrane is slightly more hydrophilic than the PES membrane, while it is more hydrophobic than PES-PVP and PES-CNF1 membranes. This is thought to be due to the inability of CNF to exhibit a good distribution in the membrane structure due to the excessive increase in viscosity because the membrane casting solution contains PES, PVP, and a high amount (1% wt.) of CNF together [31,72]. The inability to take advantage of the interaction between –OH groups and water molecules in the structures of poorly dispersed CNF cause a decrease in membrane surface hydrophilicity. Similarly, the viscosity and surface hydrophobicity of the PES-PVP-CNF0.5 membrane is higher than the casting solution since the PES-PVP CNF1 membrane casting solution contains a more considerable amount of CNF. In addition, the denser surface of the PES-CNF1 membrane than the other membranes causes the contact angle to be higher.

3.5. Water content of membranes

Apart from the contact angle, another parameter that indicates the hydrophilicity of the membrane is the membranes' water content. Fig. 7 shows the results of the water content of the membranes. The lowest water content is obtained in the PES membrane, with 71%. The water content of PES-PVP, PES-CNF0.5, and PES-CNF1 increases by 14%, 7%, and 9%, respectively, compared to the PES membrane. Since the inclusion of hydrophilic materials in the PES membrane increases the membrane surface porosity, the adsorption and penetration of water into the membrane become easier, and the water content increases. In addition, hydrogen bonding between –OH groups in CNF and water molecules increases water content.

The water content of the PES-PVP-CNF0.5 membrane is 1.4% and 8.2% higher, respectively, compared to the PES-PVP and PES-CNF0.5 membranes. Similarly, the water content of the PES-PVP-CNF1 membrane is 1.9% and 6.7% higher than the PES-PVP and PES-CNF1 membranes, respectively. The results reveal that PVP plays a unique role in the membrane compared to CNF in terms of

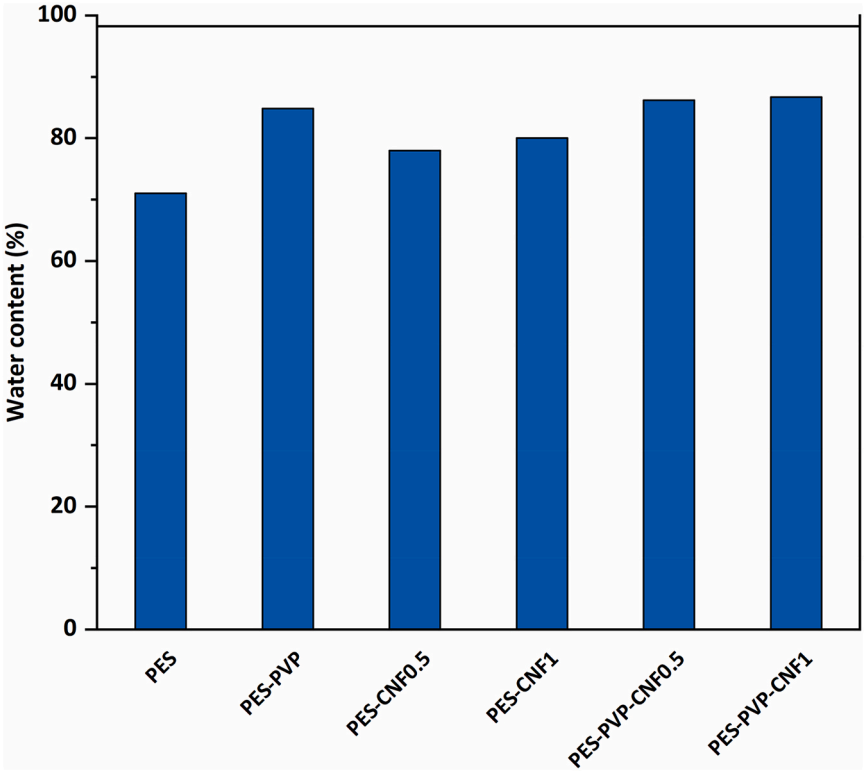

Fig. 7. The measured and averaged water content of the membranes.

increasing the water content of the membrane. The highest water content is obtained in the PES-PVP-CNF1 membrane (86.7%), followed by the PES-PVP-CNF0.5 (86.2%) membrane. The fact that the PES-PVP-CNF1 membrane has a less porous interior despite the higher CNF content prevented the PES-PVP-CNF1 membrane from having a much higher water content than the PES-PVP-CNF0.5 membrane.

3.6. Porosity and mean pore size

Pressure-driven membranes used in water/wastewater treatment are commonly categorised into four classes: microfiltration, UF, nanofiltration, and reverse osmosis, respectively, according to their decreasing pore sizes. The porosity and mean pore size results of the membranes are given in Fig. 8. The mean pore sizes of the prepared membranes are in the range of 18.4–21.9 nm, which is characteristic of UF membranes (1–100 nm). The primary mechanism for removing contaminants from water/wastewater using porous UF membranes is size exclusion, and contaminants larger than the pore size of UF membranes are retained by accumulating on the membrane surface and pores. In comparison, contaminants smaller than the pore size may pass through the membrane. UF membranes prepared in this study can be used to remove colour, turbidity, suspended solids, organic substances, bacteria, and viruses from water/wastewater. In addition, the prepared membranes can be used before nanofiltration and reverse osmosis membranes used in drinking water/wastewater treatment to reduce the contaminant load of these membranes and prevent them from easily clogging. The porosity and mean pore size of the neat PES membrane are determined as 55% and 18.4 nm, respectively. PVP, CNF, and PVP-CNF-doped membranes have higher porosity and mean pore size than neat PES membranes. By incorporating hydrophilic PVP and CNF into the membrane casting solution, thermodynamic instability during phase inversion is improved, and membranes with higher porosity and mean pore size are obtained. The porosity and mean pore size increase due to the increased amount of CNF in the PES-CNF membranes, increasing the exchange rate during phase inversion. Similarly, Ding et al. show that porosity and pore size increase by adding 0.8% wt. CNF to the polysulfone membrane [27].

The greatest porosity and largest mean pore size are obtained in the PES-PVP-CNF0.5 membrane. The porosity and mean pore size of the PES-PVP and PES-CNF0.5 membrane are 74% and 20 nm and 59% and 18.6 nm, respectively, while the porosity and mean pore size of the PES-PVP-CNF0.5 membrane are found 83% and 21.9 nm. The results show that the combined effect of PVP and CNF provides superior performance in increasing membrane porosity than the effect separately. On the other hand, the porosity of the PES PVP-CNF1 membrane is lower than PES-PVP, PES-CNF1, and PES-PVP CNF0.5 membranes. Since the high amount of CNF (1% wt.) and PVP cause the viscosity of the membrane casting solution to increase excessively, the exchange rate decreases during phase inversion and a less porous dense structure are obtained. In addition, its high viscosity causes CNFs not to be well dispersed in the casting solution, which contributes to the reduction of porosity and average pore size.

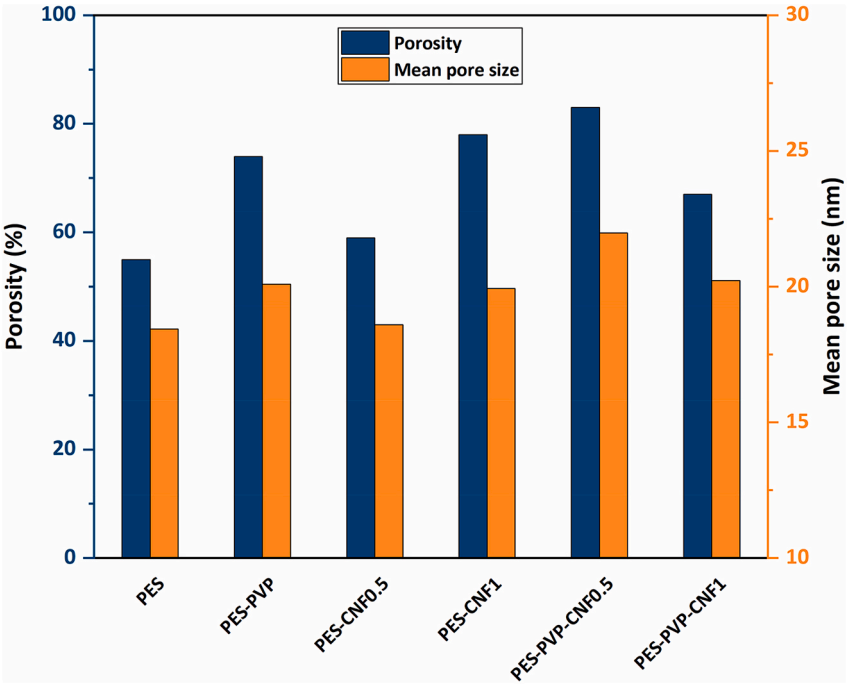

Fig. 8. Porosity and mean pore size of membranes.

3.7. Pure water flux

For good performance, polymeric membranes used in water/wastewater treatment are required to exhibit high flux performance in addition to having high contaminant removal efficiency. Pure water fluxes of the membranes under 0.3 MPa pressure are shown in Fig. 9. The flux of the neat PES membrane is 221.2 L/m^2. h. The pure water flux of the PES membrane increases by about 10% with the addition of PVP and increases to 245.3 L/m^2. h. Since PVP increases the membrane surface hydrophilicity, porosity, and mean pore size, an increase in the flux of the PES membrane with the addition of PVP is seen. With the addition of 0.5% and 1% wt. of CNF to the PES membrane, the pure water flux increases by 4% and 33%, respectively. The higher porosity, pore size, and surface hydrophilicity of the PES-CNF1 membrane compared to the PES-CNF0.5 membrane contribute to a greater increase in the pure water flux of the PES membrane with the addition of 1% CNF. The highest pure water flux is obtained with 373.7 L/m^2. h in the PES-PVP-CNF0.5 membrane. High water flux performance reduces the pressure required for water to pass through the membranes and the membrane area in pressure-driven membranes, thus reducing energy and membrane costs, respectively. Since the PES-PVP-CNF0.5 membrane has the highest pure water flux, the desired flux performance can be achieved using less energy and/or less membrane area with the PES-PVP-CNF0.5 membrane compared to other membranes under the same conditions. As opposed to that, the pure water flux of the PES-PVP-CNF1 membrane has the lowest flux (217 L/m^2. h) among all membranes. This result shows that if PVP and CNF increase the membrane casting solution's viscosity excessively, the membrane surface hydrophilicity and porosity will decrease, resulting in denser membranes with high hydraulic resistance that prevent water passage.

3.8. Mechanical characterisation and modelling

The scope of this study includes the investigation of the effects of wet and dry conditions, particle reinforcements, and the pore-forming polymer PVP on the mechanics of the membranes. For this purpose, experimental studies are conducted, and the membranes are modelled numerically. The FE analysis and Mori-Tanaka homogenisation methods are chosen for the numerical modelling process, and the tensile test is carried out for the experimental study. The results are presented and discussed in this section.

The tensile test is performed on the prepared membranes. From the results, the modulus of elasticity (E), tensile strength (σ_t), and elongation at break (also referred to as rupture strain) (ε_b) values of the tested membranes are extracted. In light of these values, the membrane's behaviour in the uniaxial tensile load is interpreted, and the results of the different samples are compared. Tensile strength and average rupture strain values of samples are also given in Figs. 10 and 11.

Furthermore, the Mori-Tanaka mean-field homogenisation and FE methods are used to predict the mechanical properties of the

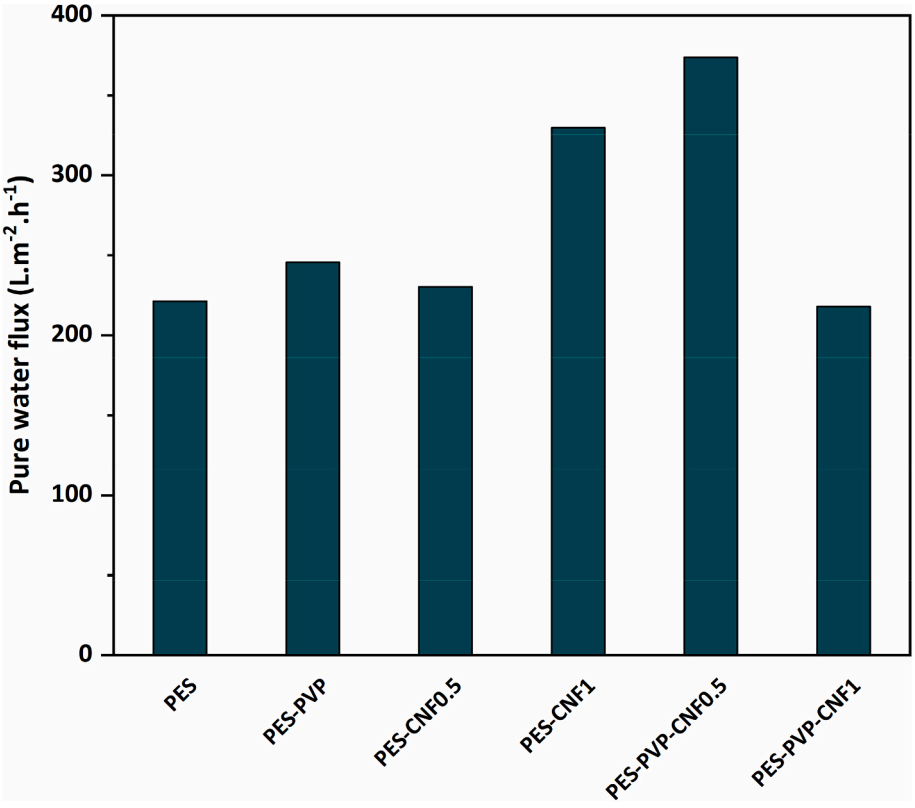

Fig. 9. The measured and averaged pure water flow of the membranes at 0.3 MPa pressure.

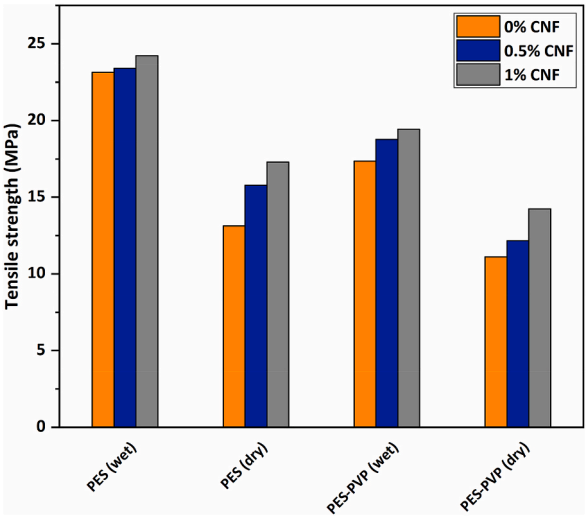

Fig. 10. Tensile strength of membranes.

membranes. Then, their results are compared to the experimental ones. The unreinforced membranes are assumed to be the matrix phase, and the impact of reinforcing CNF particles is studied. The Young's modulus values of the composite membranes are calculated by the mentioned numerical methods. The elasticity moduli of samples are determined by both experimental and numerical investigations, and they are presented in Fig. 12 together.

When the tensile properties of wet and dry samples are examined, it is seen that these samples have different mechanical characteristics. The tensile test results show that the dry samples are more rigid than the wet samples in all membrane combinations. In addition, when the elongation at break values of dry and wet samples are considered, it is seen that the elongation at break values of wet samples are greater than those of dry samples. This shows that wet samples display more ductile behaviour than dry specimens.

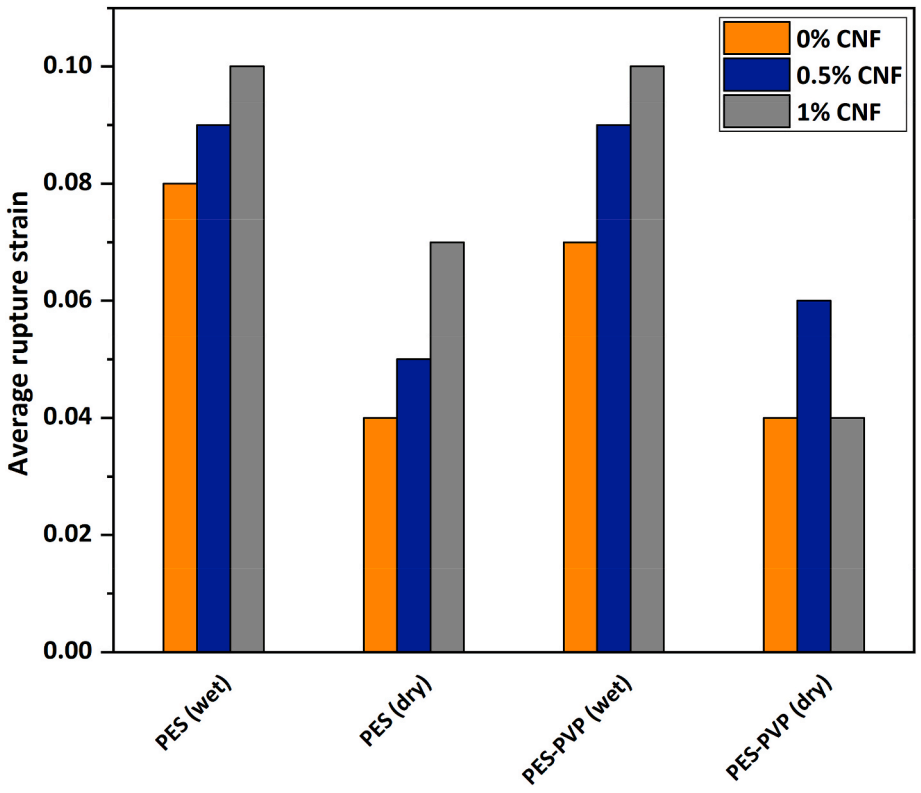

Fig. 11. Average rupture strain of membranes.

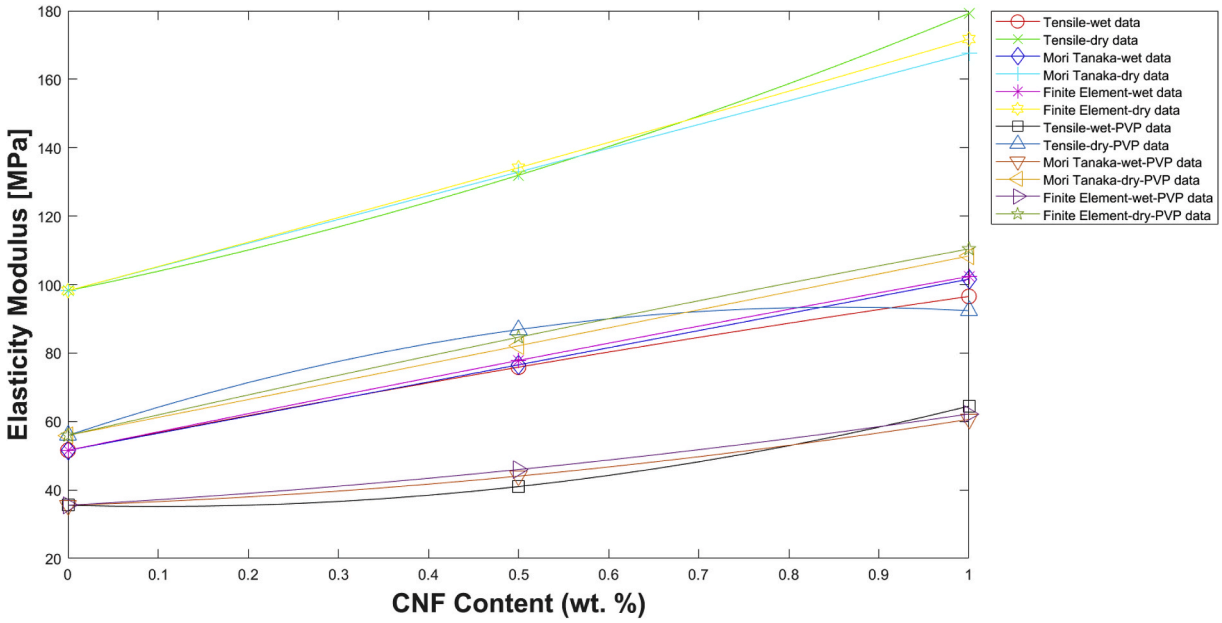

Fig. 12. The average elasticity modulus of membranes.

These results are also in good agreement with the literature [24,52,53].

In addition, it would be accurate to claim that CNF reinforcement increases the stiffness for both wet and dry samples. When the elasticity modulus of CNF particles is compared to the matrix material, it can be pointed out that this is an expected result. With the addition of CNF (0.5% and 1% wt.), an increase of 34.33% and 82.48% in experimental results, respectively, is observed for the dry condition in composite membranes with PES/NMP matrix. The tensile tests performed on wet PES/NMP membranes yield an increase due to CNF contribution of 47.1% and 87.22%, respectively. Investigating the numerical analysis results, it is to be pointed out that with growing CNF content in the membrane, greater elasticity modulus values are obtained, and the stiffer the membrane gets. Also, wet membranes are more compliant than dry membranes of the same composition.

When pore-forming polymer material (PVP) is added to the polymer (PES) matrix, it is observed that the stiffness of membranes with pure NMP solvent (membrane without PVP) is higher. This is because the PVP addition to the polymer matrix creates a more porous structure, and therefore a decrease in rigidity is observed.

Comparing the Mori-Tanaka homogenisation and FE results, the FE approach is also in good agreement with the results of Mori-

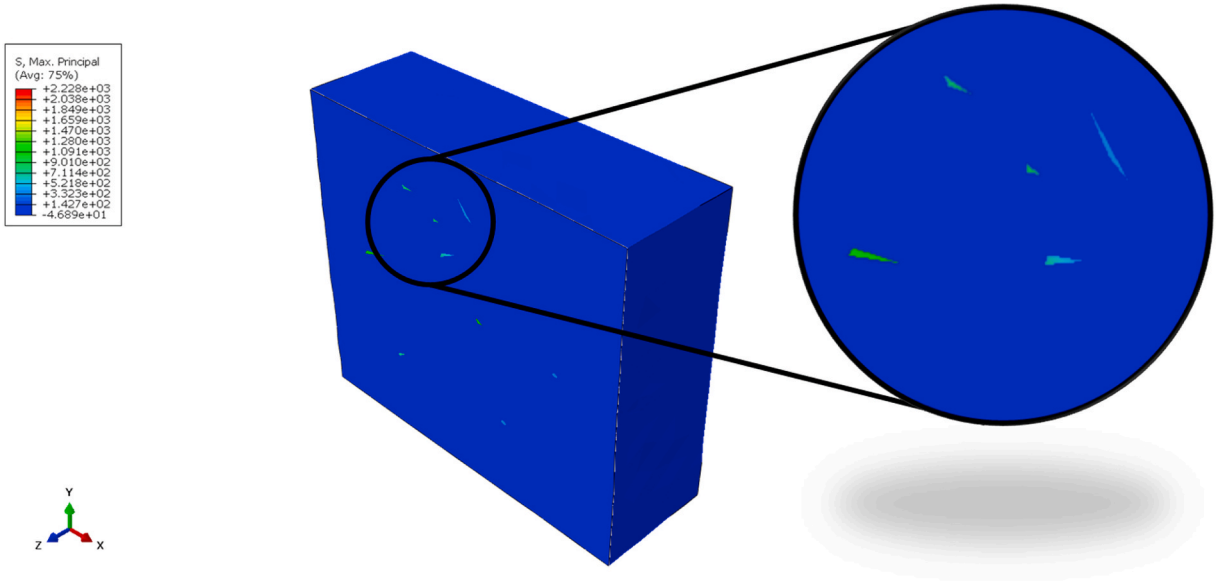

Fig. 13. Stress distribution on 1% wt. CNF-doped dry PES RVE.

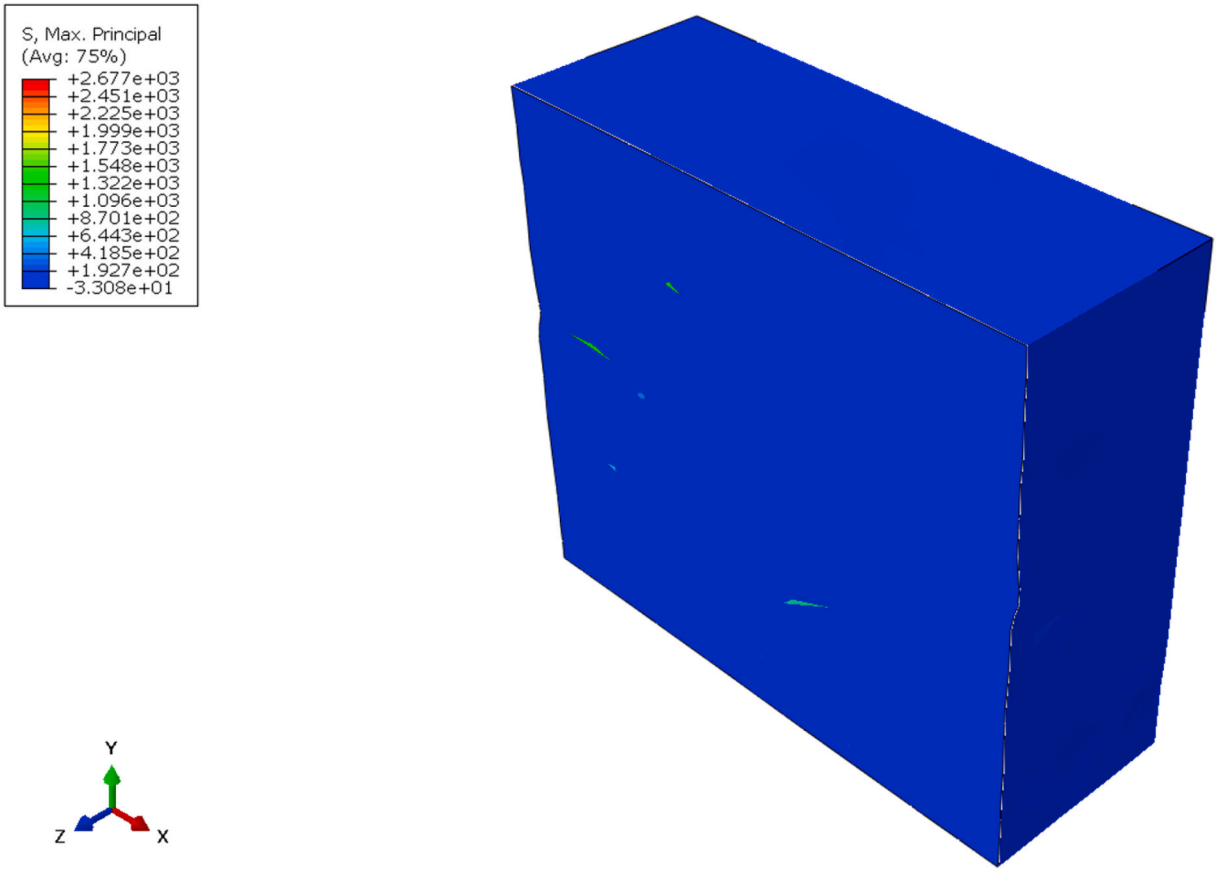

Fig. 14. Stress distribution on 1% wt. CNF-doped wet PES RVE.

Tanaka. In comparison to the experimental data, it can be shown that the stiffness values computed using FE are higher and the error rates are lower. This difference can be explained by considering that the FE approach performs a more accurate and detailed stress analysis, which better represents the material's mechanics.

Furthermore, the stress distributions obtained on the RVE from the FE analyses are also discussed in this section. The outputs of the FE models representing the stress distributions on the composite materials are shown in Figs. 13–16. Considering the stress distributions formed on the RVE, it is to be noted that the stress values in and around the particle reinforcements are higher. It is seen that the matrix phase transfers a significant amount of the load applied on the material to the particles, and the transferred load is carried by the reinforcing phase, the particles.

With FE analyses, the effects of wet and dry conditions and pore-forming agent on the stress distribution of RVE is also discussed. Samples with 1% wt. CNF content is evaluated in order to discover the effects efficiently. Firstly, with these analyses, the load-bearing capacities of wet and dry membranes are discussed. Stress distributions of 1% wt. CNF-doped dry PES, 1% wt. CNF-doped wet PES, 1% wt. CNF-doped dry PES/PVP, 1% wt. CNF-doped wet PES/PVP membranes are given in Figs. 13–16, respectively. Figs. 13–16 reveal that lower stress values are observed under the same uniaxial strain loading in wet RVEs. This is caused by dry membranes' higher stiffness/elasticity modulus than wet membranes. Also, these results agree with the experimental results.

Figs. 15 and 16 are presented to evaluate the effect of the pore-forming agent. Based on the results, an increase in maximum principal stress values is observed in wet and dry conditions. Similar to previous results, it can also be related to a decrease in the rigidity of the matrix due to the pore-forming agent, which leads to an increase in the load carried by the particles. Thus, the maximum stress values rise, which were already in the particles. Since similar findings are reached with the experimental result, FE results agree with experimental results.

4. Conclusion

In this study, PES, PES-PVP, PES-CNF, and PES-PVP-CNF membranes are manufactured by employing the method of phase inversion. The functional groups, morphology, contact angle, water content, pure water flux, porosity, mean pore size, thermal properties, and mechanical properties of the prepared membranes are characterised.

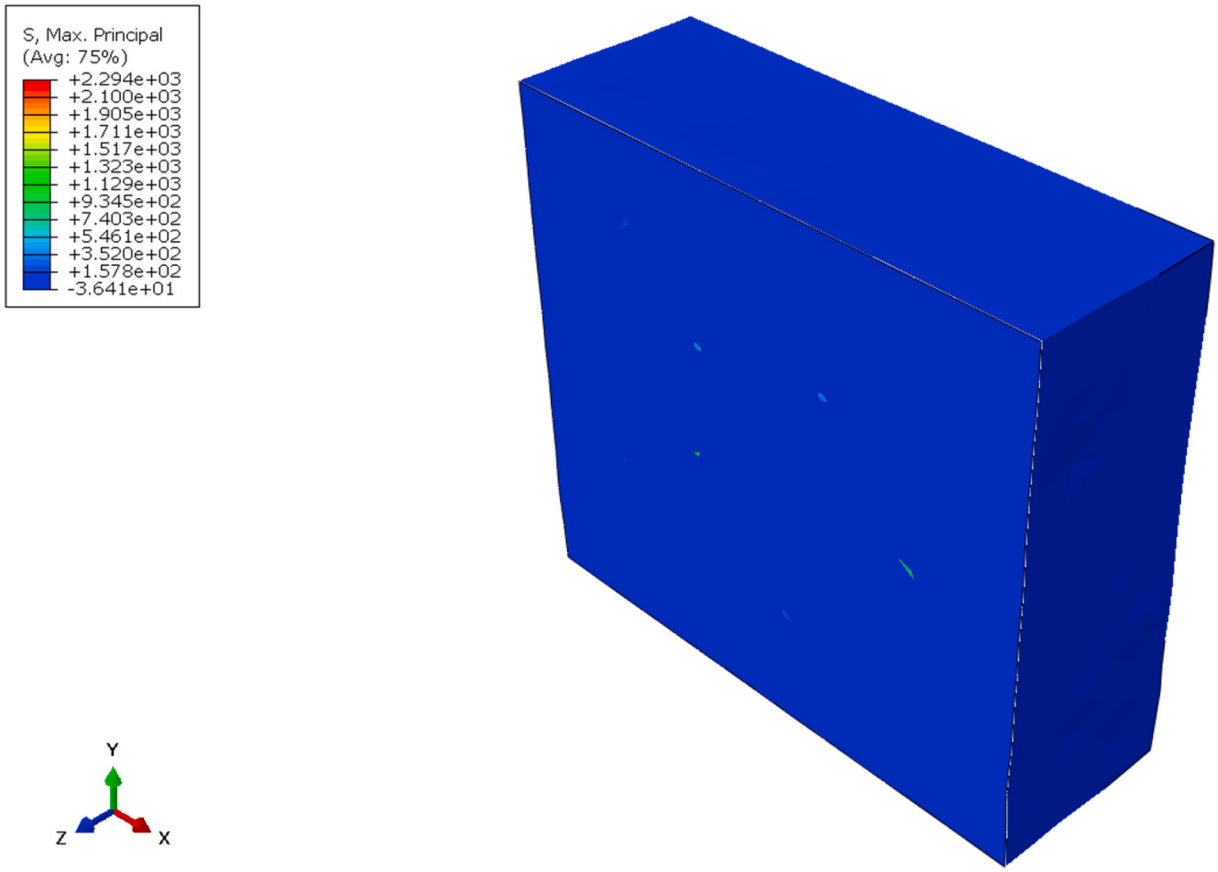

Fig. 15. Stress distribution on 1% wt. CNF-doped dry PES/PVP RVE.

- With the addition of PVP to the PES membrane, The pure water flux (~10%), water content (~14%), porosity (~19%), and mean pore size (~8%) increase, and the membrane surface hydrophilicity increases by decreasing the contact angle by approximately 9.5%.
- Adding CNF to the PES membrane and the increasing amount of CNF in the membrane, pure water flux, water content, porosity, mean pore size, and surface hydrophilicity increase. Compared to the neat PES membrane, the PES-CNF1 membrane increases the pure water flux by 33%, the water content by 9%, the porosity by 23% and the mean pore size by 7.5%, and the contact angle decrease by 10%.
- The combined addition of PVP and CNF to the PES membrane increases the pure water flux, water content, porosity, average pore size, and surface hydrophilicity of the PES membrane. Pure water flux, water content, porosity, mean pore size, and hydrophilicity values of the PES-PVP-CNF0.5 membrane are higher than the PES-PVP and PES-CNF0.5 membranes.
- The more viscous casting solution of the membrane with a combination of PVP and a high amount of CNF (1% wt.) causes the membrane to become denser and more non-porous, reducing pure water flux and surface hydrophilicity compared to the PES-PVP CNF0.5 membrane.
- The thermal behaviours of PES-based membranes are investigated, and it is observed that the PES-CNF1 membrane exhibited well thermal stability.
- From the mechanical characterisation of membranes, it can be commented that with the CNF reinforcement, membrane samples show more rigid behaviour and gets more ductile. And with PVP addition, membrane samples show less rigid behaviour.
- In addition, with the wet and dry samples, the hygrothermal conditions of samples are investigated. It is found that dry membranes show more rigid behaviour, and dry membranes are more brittle than wet membranes.
- For the modelling part of this study, two Mori-Tanaka homogenisation and FE methods are employed. More accurate results can be obtained with the FE method than Mori-Tanaka approach. Another advantage of the FE is that the stress distributions over the RVE can be obtained. However, FE analysis has a higher computational cost. It may be preferred in cases where the computational cost is not important, and the stress distribution over the RVE is necessarily to be known.

This study revealed that the undesirable conditions such as flux reduction, fouling, and low mechanical and thermal stability encountered in the treatment of drinking water, domestic wastewater, and industrial wastewater could be overcome by adding non-

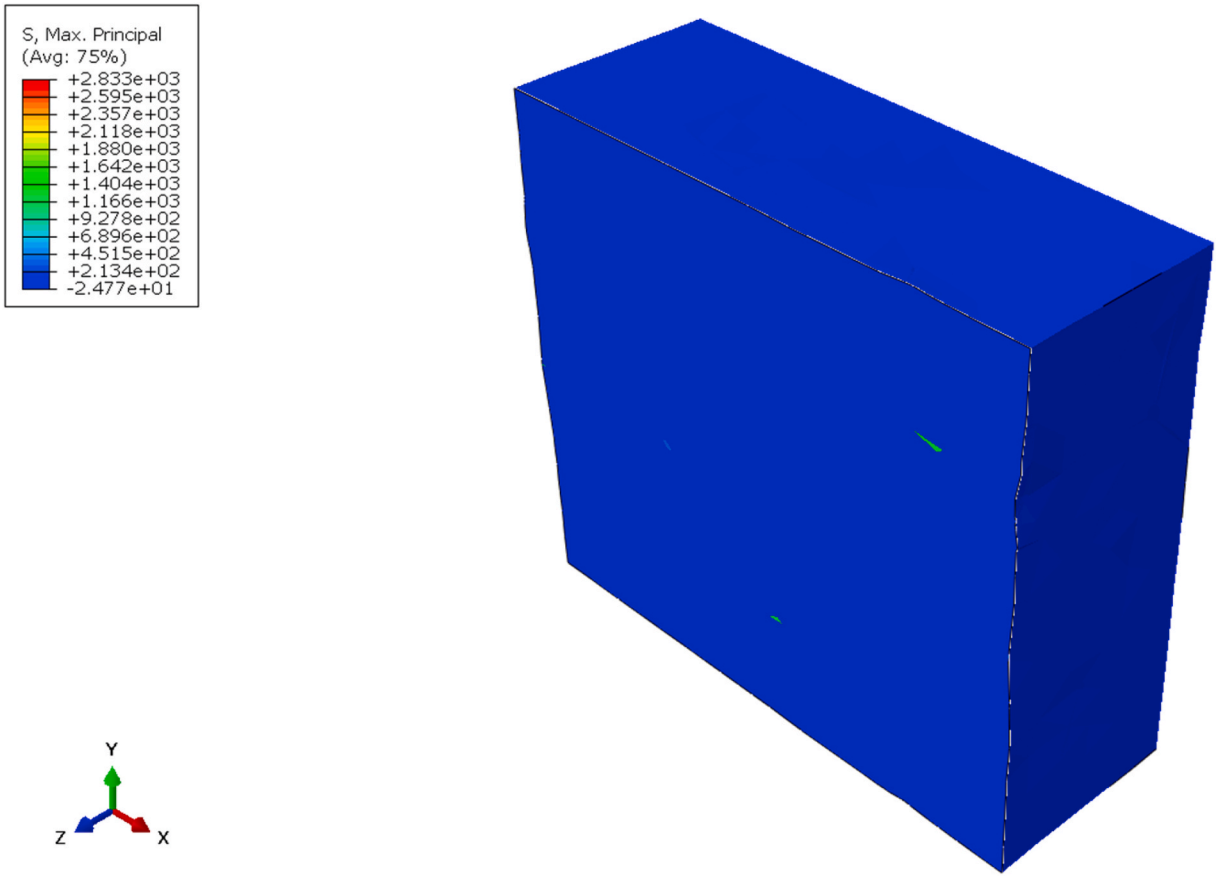

Fig. 16. Stress distribution on 1% wt. CNF-doped wet PES/PVP RVE.

toxic, renewable, biodegradable CNFs to PES-based membranes with and without PVP additives in appropriate amounts. In addition, the low cost of membrane materials used in water/wastewater treatment is an important issue. It is observed that significant improvements in membrane performance can be achieved with the addition of CNF, which is much more cost-effective than many nanomaterials (such as carbon nanotubes and some nanometal oxides) used in the preparation of nanocomposite polymer-based membranes.

Author contribution statement

Seren Acarer: Conceived and designed the experiments; Performed the experiments; Analyzed and interpreted the data; Contributed reagents, materials, analysis tools or data; Wrote the paper.

İnci Pir: Performed the experiments; Analyzed and interpreted the data; Contributed reagents, materials, analysis tools or data; Wrote the paper.

Mertol Tüfekci: Conceived and designed the experiments; Contributed reagents, materials, analysis tools or data; Wrote the paper.

Tuğba Erkoç: Performed the experiments; Analyzed and interpreted the data; Wrote the paper.

Vehbi Öztekin: Performed the experiments.

Sevgi Güneş Durak: Conceived and designed the experiments; Wrote the paper.

Mehmet Şükrü Özçoban, Güler Türkoğlu Demirkol: Contributed reagents, materials, analysis tools or data; Wrote the paper.

Moayyad Alhammod: Performed the experiments; Contributed reagents, materials, analysis tools or data.

Selva Çavuş: Conceived and designed the experiments; Performed the experiments; Analyzed and interpreted the data; Wrote the paper.

Neşe Tüfekci: Conceived and designed the experiments; Performed the experiments; Contributed reagents, materials, analysis tools or data; Wrote the paper.

Funding statement

This research was supported by Istanbul University-Cerrahpasa Scientific Research Projects Coordination Unit [Grant Number:

FYL-2021-35,671].

Data availability statement

Data included in article/supp. material/referenced in article.

References

[1] N.K. Dama, A. Szymczyk, A.A. Tamsa, B. Tchatchueng, Preparation and characterization of PES-based membranes : impact of the factors using a central composite an experimental design, Int. J. Chem. Chem. Eng. Syst. 4 (2019) 5–15.

[2] W. Wang, L. Zhu, B. Shan, C. Xie, C. Liu, F. Cui, G. Li, Preparation and characterization of SLS-CNT/PES ultrafiltration membrane with antifouling and antibacterial properties, J. Membr. Sci. 548 (2018) 459–469, https://doi.org/10.1016/j.memsci.2017.11.046.

[3] A. Taufiq, A. Nikmah, A. Hidayat, S. Sunaryono, N. Mufti, N. Hidayat, H. Susanto, Synthesis of magnetite/silica nanocomposites from natural sand to create a drug delivery vehicle, Heliyon 6 (2020), e03784, https://doi.org/10.1016/j.heliyon.2020.e03784.

[4] N. Saba, M. Jawaid, Recent Advances in Nanocellulose-Based Polymer Nanocomposites, Elsevier Ltd, 2017, https://doi.org/10.1016/B978-0-08-100957-4.00004-8.

[5] A.H. Tayeb, E. Amini, S. Ghasemi, M. Tajvidi, Cellulose nanomaterials-binding properties and applications: a review, Molecules 23 (2018) 1–24, https://doi.org/10.3390/molecules23102684.

[6] Z. Karim, A.P. Mathew, V. Kokol, J. Wei, M. Grahn, High-flux affinity membranes based on cellulose nanocomposites for removal of heavy metal ions from industrial effluents, RSC Adv. 6 (2016) 20644–20653, https://doi.org/10.1039/c5ra27059f.

[7] I. Khan, K. Saeed, I. Khan, Nanoparticles: properties, applications and toxicities, Arab. J. Chem. 12 (2019) 908–931, https://doi.org/10.1016/j.arabjc.2017.05.011.

[8] D. Trache, A.F. Tarchoun, M. Derradji, T.S. Hamidon, N. Masruchin, N. Brosse, M.H. Hussin, Nanocellulose: from Fundamentals to Advanced Applications, 2020, https://doi.org/10.3389/fchem.2020.00392.

[9] H.-Y. Yu, C.-F. Yan, Mechanical properties of cellulose nanofibril (CNF)- and cellulose nanocrystal (CNC)-based nanocomposites, in: Handbook of Nanocellulose and Cellulose Nanocomposites, 2017, pp. 393–443, https://doi.org/10.1002/9783527689972.ch12.

[10] H.F. Tan, B.S. Ooi, C.P. Leo, Future perspectives of nanocellulose-based membrane for water treatment, J. Water Proc. Eng. 37 (2020), 101502, https://doi.org/10.1016/j.jwpe.2020.101502.

[11] M. Nasir, R. Hashim, O. Sulaiman, M. Asim, Nanocellulose, in: Cellulose-Reinforced Nanofibre Composites, Elsevier, 2017, pp. 261–276, https://doi.org/10.1016/B978-0-08-100957-4.00011-5.

[12] M.Y. Khalid, A. Al Rashid, Z.U. Arif, W. Ahmed, H. Arshad, Recent advances in nanocellulose-based different biomaterials: types, properties, and emerging applications, J. Mater. Res. Technol. 14 (2021) 2601–2623, https://doi.org/10.1016/J.JMRT.2021.07.128.

[13] A. Blanco, M.C. Monte, C. Campano, A. Balea, N. Merayo, C. Negro, Nanocellulose for Industrial Use: Cellulose Nanofibers (CNF), Cellulose Nanocrystals (CNC), and Bacterial Cellulose (BC), Elsevier Inc., 2018, https://doi.org/10.1016/B978-0-12-813351-4.00005-5.

[14] P. Huang, C. Wang, Y. Huang, M. Wu, Structure and properties of cellulose nanofibrils, in: Nanocellulose, Wiley, 2019, pp. 53–80, https://doi.org/10.1002/9783527807437.ch3.

[15] A.W. Carpenter, C.F. De Lannoy, M.R. Wiesner, Cellulose nanomaterials in water treatment technologies, Environ. Sci. Technol. 49 (2015) 5277–5287, https://doi.org/10.1021/es506351r.

[16] N. Saba, M. Jawaid, Recent Advances in Nanocellulose-Based Polymer Nanocomposites, Elsevier Ltd, 2017, https://doi.org/10.1016/B978-0-08-100957-4.00004-8.

[17] H.F. Tan, B.S. Ooi, C.P. Leo, Future perspectives of nanocellulose-based membrane for water treatment, J. Water Proc. Eng. 37 (2020), 101502, https://doi.org/10.1016/j.jwpe.2020.101502.

[18] Z. Ding, X. Liu, Y. Liu, L. Zhang, Enhancing the compatibility, hydrophilicity and mechanical properties of polysulfone ultrafiltration membranes with lignocellulose nanofibrils, Polymers 8 (2016), https://doi.org/10.3390/polym8100349.

[19] J.D.P. de Amorim, K.C. de Souza, C.R. Duarte, I. da Silva Duarte, F. de Assis Sales Ribeiro, G.S. Silva, P.M.A. de Farias, A. Stingl, A.F.S. Costa, G.M. Vinhas, L. A. Sarubbo, Plant and bacterial nanocellulose: production, properties and applications in medicine, food, cosmetics, electronics and engineering. A review, Environ. Chem. Lett. 18 (2020) 851–869, https://doi.org/10.1007/s10311-020-00989-9.

[20] L. Bai, N. Bossa, F. Qu, J. Winglee, G. Li, K. Sun, H. Liang, M.R. Wiesner, Comparison of Hydrophilicity and Mechanical Properties of Nanocomposite Membranes with Cellulose Nanocrystals and Carbon Nanotubes, 2017, https://doi.org/10.1021/acs.est.6b04280.

[21] L. Bai, H. Wu, J. Ding, A. Ding, X. Zhang, N. Ren, G. Li, H. Liang, Cellulose nanocrystal-blended polyethersulfone membranes for enhanced removal of natural organic matter and alleviation of membrane fouling, Chem. Eng. J. 382 (2020), 122919, https://doi.org/10.1016/j.cej.2019.122919.

[22] J. Lv, G. Zhang, H. Zhang, F. Yang, Exploration of permeability and antifouling performance on modified cellulose acetate ultrafiltration membrane with cellulose nanocrystals, Carbohydr. Polym. 174 (2017) 190–199, https://doi.org/10.1016/j.carbpol.2017.06.064.

[23] D. Zhang, A. Karkooti, L. Liu, M. Sadrzadeh, T. Thundat, Y. Liu, R. Narain, Fabrication of antifouling and antibacterial polyethersulfone (PES)/cellulose nanocrystals (CNC) nanocomposite membranes, J. Membr. Sci. 549 (2018) 350–356, https://doi.org/10.1016/j.memsci.2017.12.034.

[24] P. Qu, H. Tang, Y. Gao, L.P. Zhang, S. Wang, Polyethersulfone composite membrane blended with cellulose fibrils, Bioresources 5 (2010) 2323–2336.

[25] N. Li, J. Zheng, P. Hadi, M. Yang, X. Huang, H. Ma, H.W. Walke, B.S. Hsiao, Synthesis and characterization of a high flux nanocellulose–cellulose acetate nanocomposite membrane, Membranes 9 (2019), https://doi.org/10.3390/membranes9060070.

[26] W. Zhang, L. Zhong, T. Wang, Z. Jiang, X. Gao, L. Zhang, Surface modification of cellulose nanofibers and their effects on the morphology and properties of polysulfone membranes, IOP Conf. Ser. Mater. Sci. Eng. 397 (2018), https://doi.org/10.1088/1757-899X/397/1/012016.

[27] Z. Ding, X. Liu, Y. Liu, L. Zhang, Enhancing the compatibility, hydrophilicity and mechanical properties of polysulfone ultrafiltration membranes with lignocellulose nanofibrils, Polymers 8 (2016), https://doi.org/10.3390/polym8100349.

[28] J. Lv, G. Zhang, H. Zhang, F. Yang, Graphene oxide-cellulose nanocrystal (GO-CNC) composite functionalized PVDF membrane with improved antifouling performance in MBR: behavior and mechanism, Chem. Eng. J. 352 (2018) 765–773, https://doi.org/10.1016/j.cej.2018.07.088.

[29] J. Lv, G. Zhang, H. Zhang, C. Zhao, F. Yang, Improvement of antifouling performances for modified PVDF ultrafiltration membrane with hydrophilic cellulose nanocrystal, Appl. Surf. Sci. 440 (2018) 1091–1100, https://doi.org/10.1016/j.apsusc.2018.01.256.

[30] C. Balcik-Canbolat, B. Van der Bruggen, Efficient removal of dyes from aqueous solution: the potential of cellulose nanocrystals to enhance PES nanocomposite membranes, Cellulose 27 (2020) 5255–5266, https://doi.org/10.1007/s10570-020-03157-y.

[31] L. Cristina Battirola, Patrícia Fernanda Andrade, Gabriela Vollet Marson, Miriam Dupas Hubinger, Maria do Carmo Gonçalves, Cellulose acetate/cellulose nanofiber membranes for whey and fruit juice microfiltration, Cellulose. 24 (n.d.). https://doi.org/10.1007/s10570-017-1510-8.

[32] L. Bai, H. Wu, J. Ding, A. Ding, X. Zhang, N. Ren, G. Li, H. Liang, Cellulose nanocrystal-blended polyethersulfone membranes for enhanced removal of natural organic matter and alleviation of membrane fouling, Chem. Eng. J. 382 (2020), 122919, https://doi.org/10.1016/j.cej.2019.122919.

[33] N. Li, J. Zheng, P. Hadi, M. Yang, X. Huang, H. Ma, H.W. Walke, B.S. Hsiao, Synthesis and characterization of a high flux nanocellulose–cellulose acetate nanocomposite membrane, Membranes 9 (2019), https://doi.org/10.3390/membranes9060070.

[34] V.H. Tran, J.-D. Kim, J.-H. Kim, S.-K. Kim, J.-M. Lee, Influence of cellulose nanocrystal on the cryogenic mechanical behavior and thermal conductivity of polyurethane composite, J. Polym. Environ. 28 (2020) 1169–1179, https://doi.org/10.1007/s10924-020-01673-3.

[35] L. Kong, D. Zhang, Z. Shao, B. Han, Y. Lv, K. Gao, X. Peng, Superior effect of TEMPO-oxidized cellulose nanofibrils (TOCNs) on the performance of cellulose triacetate (CTA) ultrafiltration membrane, Desalination 332 (2014) 117–125, https://doi.org/10.1016/j.desal.2013.11.005.

[36] C.M. Ewulonu, J.L. Chukwuneke, I.C. Nwuzor, C.H. Achebe, Fabrication of cellulose nanofiber/polypyrrole/polyvinylpyrrolidone aerogels with box-Behnken design for optimal electrical conductivity, Carbohydr. Polym. 235 (2020), 116028, https://doi.org/10.1016/J.CARBPOL.2020.116028.

[37] P. Franco, I. De Marco, The use of poly(N-vinyl pyrrolidone) in the delivery of drugs: a review, Polymers 12 (2020) 1114, https://doi.org/10.3390/POLYM12051114.

[38] M. Voronova, N. Rubleva, N. Kochkina, A. Afineevskii, A. Zakharov, O. Surov, Preparation and characterization of polyvinylpyrrolidone/cellulose nanocrystals composites, Nanomaterials 8 (2018) 1011, https://doi.org/10.3390/NANO8121011.

[39] B. Jaleh, E. Zare, S. Azizian, O. Qanati, M. Nasrollahzadeh, R.S. Varma, Preparation and characterization of polyvinylpyrrolidone/polysulfone ultrafiltration membrane modified by graphene oxide and titanium dioxide for enhancing hydrophilicity and antifouling properties, J. Inorg. Organomet. Polym. Mater. 30 (2020) 2213–2223, https://doi.org/10.1007/S10904-019-01367-X/TABLES/2.

[40] F. Rafieian, M. Mousavi, A. Dufresne, Q. Yu, Polyethersulfone membrane embedded with amine functionalized microcrystalline cellulose, Int. J. Biol. Macromol. 164 (2020) 4444–4454, https://doi.org/10.1016/J.IJBIOMAC.2020.09.017.

[41] R.A. Milescu, C.R. McElroy, T.J. Farmer, P.M. Williams, M.J. Walters, J.H. Clark, Fabrication of PES/PVP water filtration membranes using Cyrene®, a safer bio-based polar aprotic solvent, Adv. Polym. Technol. 2019 (2019), 9692859, https://doi.org/10.1155/2019/9692859.

[42] T. Marino, F. Galiano, S. Simone, A. Figoli, DMSO EVOL^{TM} as novel non-toxic solvent for polyethersulfone membrane preparation, Environ. Sci. Pollut. Control Ser. 26 (2019) 14774–14785, https://doi.org/10.1007/S11356-018-3575-9/TABLES/7.

[43] X. Ren, H. Li, K. Liu, H. Lu, J. Yang, R. He, Preparation and investigation of reinforced PVP blend membranes for high temperature polymer electrolyte membranes, Fibers Polym. 19 (2019) 2449–2457, https://doi.org/10.1007/S12221-018-8361-2.

[44] K. Wang, A.A. Abdalla, M.A. Khaleel, N. Hilal, M.K. Khraisheh, Mechanical properties of water desalination and wastewater treatment membranes, Desalination 401 (2017) 190–205, https://doi.org/10.1016/j.desal.2016.06.032.

[45] M. Tüfekci, S.G. Durak, İ. Pir, T.O. Acar, G.T. Demirkol, N. Tüfekci, Manufacturing, characterisation and mechanical analysis of polyacrylonitrile membranes, Polymers 12 (2020) 1–21, https://doi.org/10.3390/polym12102378.

[46] S. Acarer, İ. Pir, M. Tüfekci, G. Türkoğlu Demirkol, N. Tüfekci, Manufacturing and characterisation of polymeric membranes for water treatment and numerical investigation of mechanics of nanocomposite membranes, Polymers 13 (2021), https://doi.org/10.3390/polym13101661.

[47] A.A. Alshahrani, I.H. Alsohaimi, S. Alshehri, A.R. Alawady, M.R. El-Aassar, L.D. Nghiem, M. in het Panhuis, Nanofiltration membranes prepared from pristine and functionalised multiwall carbon nanotubes/biopolymer composites for water treatment applications, J. Mater. Res. Technol. 9 (2020) 9080–9092, https://doi.org/10.1016/J.JMRT.2020.06.055.

[48] M.A. Ruz-Cruz, P.J. Herrera-Franco, E.A. Flores-Johnson, M.V. Moreno-Chulim, L.M. Galera-Manzano, A. Valadez-González, Thermal and mechanical properties of PLA-based multiscale cellulosic biocomposites, J. Mater. Res. Technol. 18 (2022) 485–495, https://doi.org/10.1016/J.JMRT.2022.02.072.

[49] M. Alhijazi, · Babak Safaei, Q. Zeeshan, · Mohammed Asmael, · Mohammad Harb, Z. Qin, An Experimental and Metamodeling Approach to Tensile Properties of Natural Fibers Composites, (n.d.). https://doi.org/10.1007/s10924-022-02514-1.

[50] J. Fuller, S. Mitchell, T. Pozegic, X. Wu, M. Longana, M. Wisnom, Experimental evaluation of hygrothermal effects on pseudo-ductile thin ply angle-ply carbon/epoxy laminates, Compos. B Eng. 227 (2021), 109388, https://doi.org/10.1016/J.COMPOSITESB.2021.109388.

[51] K. Kumar Mahato, K. Dutta, B. Chandra Ray, Static and Dynamic Behavior of Fibrous Polymeric Composite Materials at Different Environmental Conditions, J. Polym. Environ.. 26 (1234) 1024–1050. https://doi.org/10.1007/s10924-017-1001-x.

[52] P. Raz, T. Brosh, G. Ronen, H. Tal, Tensile properties of three selected collagen membranes, BioMed Res. Int. 2019 (2019), 5163603, https://doi.org/10.1155/2019/5163603.

[53] R. Soni, T.-A. Asoh, H. Uyama, Cellulose nanofiber reinforced starch membrane with high mechanical strength and durability in water, Carbohydr. Polym. 238 (2020), 116203, https://doi.org/10.1016/j.carbpol.2020.116203.

[54] M.A. Muflikhun, M.C. Frommelt, M. Farman, A.Y. Chua, G.N.C. Santos, Structures, mechanical properties and antibacterial activity of Ag/TiO 2 nanocomposite materials synthesized via HVPG technique for coating application, Heliyon 5 (2019), e01475, https://doi.org/10.1016/j.heliyon.2019.e01475.

[55] R. Sigwadi, M.S. Dhlamini, T. Mokrani, F. Nemavhola, Enhancing the mechanical properties of zirconia/Nafion® nanocomposite membrane through carbon nanotubes for fuel cell application, Heliyon 5 (2019), e02112, https://doi.org/10.1016/j.heliyon.2019.e02112.

[56] S. Das Lala, S. Sadikbasha, A.B. Deoghare, Prediction of elastic modulus of polymer composites using Hashin–Shtrikman bound, mean field homogenization and finite element technique, Proc. Inst. Mech. Eng. C J. Mech. Eng. Sci. 234 (2020) 1653–1659, https://doi.org/10.1177/0954406219895791.

[57] S. Banerjee, B.V. Sankar, Mechanical properties of hybrid composites using finite element method based micromechanics, Compos. B Eng. 58 (2014) 318–327, https://doi.org/10.1016/J.COMPOSITESB.2013.10.065.

[58] G.D. Seidel, D.C. Lagoudas, Micromechanical analysis of the effective elastic properties of carbon nanotube reinforced composites, Mech. Mater. 38 (2006) 884–907, https://doi.org/10.1016/j.mechmat.2005.06.029.

[59] S. David Müzel, E. Pires Bonhin, N.M. Guimarães, E.S. Guidi, Polymers Application of the Finite Element Method in the Analysis of Composite Materials: A Review, (n.d.). https://doi.org/10.3390/polym12040818.

[60] M. Alhijazi, · Babak Safaei, Q. Zeeshan, · Mohammed Asmael, · Mohammad Harb, Z. Qin, An Experimental and Metamodeling Approach to Tensile Properties of Natural Fibers Composites, (n.d.). https://doi.org/10.1007/s10924-022-02514-1.

[61] M. Tüfekci, B. Özkal, C. Maharaj, H. Liu, J.P. Dear, L. Salles, Strain-rate-dependent mechanics and impact performance of epoxy-based nanocomposites, Compos. Sci. Technol. 233 (2023), 109870, https://doi.org/10.1016/j.compscitech.2022.109870.

[62] F.F. Ghiggi, L.D. Pollo, N.S.M. Cardozo, I.C. Tessaro, Preparation and characterization of polyethersulfone/N-phthaloyl-chitosan ultrafiltration membrane with antifouling property, Eur. Polym. J. 92 (2017) 61–70, https://doi.org/10.1016/j.eurpolymj.2017.04.030.

[63] S. Parani, O.S. Oluwafemi, Fabrication of superhydrophobic polyethersulfone-ZnO rods composite membrane, Mater. Lett. 281 (2020), 128663, https://doi.org/10.1016/j.matlet.2020.128663.

[64] B. Vatsha, J.C. Ngila, R.M. Moutloali, Preparation of antifouling polyvinylpyrrolidone (PVP 40K) modified polyethersulfone (PES) ultrafiltration (UF) membrane for water purification, Phys. Chem. Earth 67–69 (2014) 125–131, https://doi.org/10.1016/j.pce.2013.09.021.

[65] H. Abdul Mannan, H. Mukhtar, M. Shima Shaharun, M. Roslee Othman, T. Murugesan, Polysulfone/poly(ether sulfone) blended membranes for CO2 separation, J. Appl. Polym. Sci. 133 (2016), https://doi.org/10.1002/app.42946.

[66] MdW. Ahmad, B. Dey, A.K.A. Al Saidi, A. Choudhury, Functionalized-graphene reinforced polyethersulfone nanocomposites with improved physical and mechanical properties, Polym. Compos. 41 (2020) 4104–4116, https://doi.org/10.1002/pc.25697.

[67] G.D. Ulrich, R. Faez, Thermal, mechanical and physical properties of composite films developed from seaweed polysaccharides/cellulose nanofibers, J. Polym. Environ. 30 (2022) 3688–3700, https://doi.org/10.1007/s10924-022-02459-5.

[68] Y. Cao, Y. Jiang, Y. Song, S. Cao, M. Miao, X. Feng, J. Fang, L. Shi, Combined bleaching and hydrolysis for isolation of cellulose nanofibrils from waste sackcloth, Carbohydr. Polym. 131 (2015) 152–158, https://doi.org/10.1016/j.carbpol.2015.05.063.

[69] M. Dominic, R. Joseph, P.M.S. Begum, M. Joseph, D. Padmanabhan, L.A. Morris, A.S. Kumar, K. Formela, Cellulose nanofibers isolated from the cuscuta reflexa plant as a green reinforcement of natural rubber, Polymers 12 (2020), https://doi.org/10.3390/polym12040814.

[70] A.L. Saroj, R.K. Singh, S. Chandra, Studies on polymer electrolyte poly(vinyl) pyrrolidone (PVP) complexed with ionic liquid: effect of complexation on thermal stability, conductivity and relaxation behaviour, Mater. Sci. Eng., B 178 (2013) 231–238, https://doi.org/10.1016/j.mseb.2012.11.007.

[71] H. Bian, Y. Yang, P. Tu, J.Y. Chen, Value-added utilization of wheat straw: from cellulose and cellulose nanofiber to all-cellulose nanocomposite film, Membranes 12 (2022), https://doi.org/10.3390/membranes12050475.

[72] S. Mansur, M.H.D. Othman, A.F. Ismail, M.N. Zainol Abidin, N. Said, G.P. Sean, H. Hasbullah, S.H. Sheikh Abdul Kadir, F. Kamal, Study on the effect of spinning conditions on the performance of PSf/PVP ultrafiltration hollow fiber membrane, Malays. J. Fundam. Appl. Sci. 14 (2018) 343–347, https://doi.org/10.11113/mjfas.v14n3.1215.

[73] L.G. Tiron, M. Vlad, Baltă, research on hydrophilic nature of polyvinylpyrrolidone on polysulfone membrane filtration, IOP Conf. Ser. Mater. Sci. Eng. 374 (2018), https://doi.org/10.1088/1757-899X/374/1/012059.
[74] T. Anokhina, A. Raeva, S. Makaev, I. Borisov, V. Vasilevsky, A. Volkov, Express method of preparation of hollow fiber membrane samples for spinning solution optimization: polysulfone as example, Membranes 11 (2021), https://doi.org/10.3390/membranes11060396.
[75] U.M. Subramanian, S.V. Kumar, N. Nagiah, U.T. Sivagnanam, Fabrication of polyvinyl alcohol-polyvinylpyrrolidone blend scaffolds via electrospinning for tissue engineering applications, Int. J. Polym. Mater. Polym. Biomater. 63 (2014) 476–485, https://doi.org/10.1080/00914037.2013.854216.
[76] N.F.D. Junaidi, N.H. Othman, M.Z. Shahruddin, N.H. Alias, W.J. Lau, A.F. Ismail, Effect of graphene oxide (GO) and polyvinylpyrollidone (PVP) additives on the hydrophilicity of composite polyethersulfone (PES) membrane, Malays. J. Fundam. Appl. Sci. 15 (2019) 361–366, https://doi.org/10.11113/mjfas.v15n3.1209.